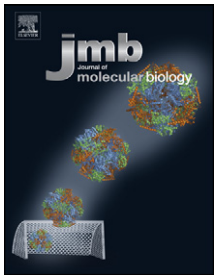

The RavA-ViaA Chaperone-Like System Interacts with and Modulates the Activity of the Fumarate Reductase Respiratory Complex

Keith S. Wong [1,†], Vaibhav Bhandari [1,†], Sarath Chandra Janga [2] and Walid A. Houry [1,3]

*1 - **Department of Biochemistry,** University of Toronto, Toronto, Ontario, M5G 1M1, Canada*
*2 - **Department of Biohealth Informatics,** School of Informatics and Computing, Indiana University Purdue University, Indianapolis, IN 46202, USA*
*3 - **Department of Chemistry,** University of Toronto, Toronto, Ontario, M5S 3H6, Canada*

***Correspondence to Walid A. Houry:** Department of Biochemistry, Faculty of Medicine, University of Toronto, MaRS Centre, West Tower, 661 University Avenue, Suite 1600, Toronto, Ontario M5G 1M1, Canada. walid.houry@utoronto.ca*
http://dx.doi.org/10.1016/j.jmb.2016.12.008
Edited by Charalampo Kalodimos

Abstract

*R*egulatory *A*TPase *v*ariant *A* (RavA) is a MoxR AAA+ protein that functions together with a partner protein that we termed *V*WA *i*nteracting with *A*AA+ *A*TPase (ViaA) containing a von Willebrand Factor A domain. However, the functional role of RavA-ViaA in the cell is not yet well established. Here, we show that RavA-ViaA are functionally associated with anaerobic respiration in *Escherichia coli* through interactions with the fumarate reductase (Frd) electron transport complex. Expression analysis of *ravA* and *viaA* genes showed that both proteins are co-expressed with multiple anaerobic respiratory genes, many of which are regulated by the anaerobic transcriptional regulator Fnr. Consistently, the expression of both *ravA* and *viaA* was found to be dependent on Fnr in cells grown under oxygen-limiting condition. ViaA was found to physically interact with FrdA, the flavin-containing subunit of the Frd complex. Both RavA and the Fe–S-containing subunit of the Frd complex, FrdB, regulate this interaction. Importantly, Frd activity was observed to increase in the absence of RavA and ViaA. This indicates that RavA and ViaA modulate the activity of the Frd complex, signifying a potential regulatory chaperone-like function for RavA-ViaA during bacterial anaerobic respiration with fumarate as the terminal electron acceptor.

Introduction

The MoxR family of AAA+ ATPases is relatively unknown, although it is diverse and widespread among bacteria and archaea [1]. The experimental evidence gathered on various MoxR proteins suggests that they have regulatory and chaperone-like roles in the maturation of protein complexes participating in a variety of biological processes including metabolism, cell morphology and development, tolerance against various types of stress, and pathogenesis [1–4]. A characteristic of the MoxR AAA+ ATPases is that their genes co-occur in close proximity with one or more genes whose proteins contain the von Willebrand factor A (VWA) domain [1]. The VWA domain features the conserved MIDAS (*m*etal *i*on-*d*ependent *a*dhesion *s*ite) motif, which binds a single divalent cation, usually Mg^{2+}, and mediates protein–protein interactions [5].

The functional characterization of the MoxR protein *r*egulatory *A*TPase *v*ariant *A* (RavA) and its corresponding VWA protein *V*WA *i*nteracting with *A*AA+ *A*TPase (ViaA) in *Escherichia coli* is an ongoing effort in our laboratory. RavA belongs to the eponymous RavA subfamily of the MoxR family [1]. The *ravA* and *viaA* genes are organized in a pattern that is typical of this subfamily with *ravA* positioned immediately upstream of *viaA* and with both genes forming a single operon [6]. In aerobically grown cells, the *ravAviaA* operon is induced by the stationary phase sigma factor, σ^S [6]. RavA has been characterized

extensively by our group both biochemically and biophysically. It forms a hexameric complex [6,7], which is typical for most AAA+ ATPases [8]. *In vitro*, the ATPase activity of RavA is optimal at neutral pH and 37 °C, which is enhanced in the presence of ViaA [6]. In stationary phase cells, RavA was found to mainly localize to the cytoplasm, while ViaA was found to be localized to both the cytoplasm and the inner membrane [9].

Although little is known about their cellular function, several interaction partners for RavA have been identified that suggest its involvement in potential regulatory roles in different biological processes. For example, RavA associates with and modulates the activity of the inducible lysine decarboxylase (LdcI) [6,7,10,11], a major acid stress response protein in *E. coli* [10,12]. The alarmone, ppGpp, was found to bind and inhibit the activity of LdcI, and the interaction of RavA with LdcI prevented this binding of ppGpp to LdcI [7]. This supports a potential role of RavA, and possibly ViaA, in bacterial acid stress response [7]. In addition, RavA and ViaA were functionally linked to bacterial respiration when they were shown to sensitize the cell to aminoglycosides [9,13]. The identification of null mutations that suppressed this phenotype, and subsequent immunoprecipitation experiments, revealed that RavA and ViaA interact with specific subunits of the NADH:ubiquinone oxidoreductase I (Nuo complex) [9]. The Nuo complex, commonly known as Complex I, is a major player in the aerobic respiration of *E. coli* [14,15]. It is also important in anaerobic respiration utilizing fumarate and dimethylsulfoxide [16].

High-throughput studies have revealed functional links between RavA-ViaA and several pathways that are directly or indirectly related to bacterial respiration. These include iron–sulfur (Fe–S) cluster biosynthesis, iron transport, and anaerobic electron transport [9,17]. In this study, we present evidence that supports a regulatory role of the RavA-ViaA proteins in the activity of the anaerobic respiratory complex fumarate reductase (Frd). The *E. coli* Frd complex catalyzes the final step of anaerobic respiration when fumarate acts as the terminal electron acceptor [18]. The complex is formed by four subunits (FrdABCD) [19,20] with FrdC and FrdD being the membrane-spanning subunits, while the flavoprotein FrdA and the iron–sulfur cluster-containing protein FrdB comprise the soluble part of the complex. During anaerobic respiration, menaquinol (MQH2) in the membrane donates electrons to the Frd complex [21]. The membrane-spanning FrdCD subcomplex anchors the FrdAB components to the membrane and, along with FrdB, provides binding sites for the quinones. The electrons then traverse through the three iron–sulfur clusters present in FrdB to the flavin adenine dinucleotide (FAD) cofactor in the FrdA active site where they are used to reduce fumarate to succinate [20–23]. Here, we find ViaA to interact with free FrdA through its C-terminal VWA domain and with RavA through its N-terminal α-helical rich domain. Importantly, the interaction of RavA-ViaA with FrdA results in a decrease in Frd activity. A model of the effect of RavA-ViaA on the maturation of the Frd complex is proposed.

Results

ravA and *viaA* display similar co-expression profiles as those of the Fnr-inducible genes

We had earlier demonstrated that RavA-ViaA interact with LdcI and the Nuo complex [2,6,9]. However, given that we postulated that RavA-ViaA might have chaperone-like activity [1,2], further studies were carried out to identify new interacting partners for this system. Initially, co-expression profiling was performed to identify genes that co-express with both *ravA* and *viaA*. This approach is based on the principle that genes are organized in a network of distinct, functional modules or hubs with highly coordinated expression patterns that correspond to specific biological processes [24–27]. Thus, genes that are functionally associated have a higher likelihood of sharing common transcriptional regulatory elements and of displaying similar expression profiles in response to the same physiological signals or external environmental stimuli.

The co-expression profiles for *ravA* and *viaA* genes were constructed by data mining a public collection of 445 *E. coli* microarray datasets collected across multiple experimental conditions, and then, genes that displayed highly similar co-expression patterns with *ravA* and *viaA* were identified. Our analysis yielded a total of 62 genes that co-express with *ravA* and 56 genes that co-express with *viaA* (Fig. 1a and Table 1). Of these, 32 genes co-express with both *ravA* and *viaA*. Given that *ravA* and *viaA* are in the same operon [1,6], genes that are co-expressed with both *ravA* and *viaA* were considered as the most reliable candidates for functional association and were examined further.

One important trend uncovered in our analysis is that many of the genes that co-express with both *ravA* and *viaA* are involved in anaerobic respiration. These include *frdA*, *frdB*, and *frdC*, which encode three of the four subunits of the Frd complex (FrdABCD); *nirB* and *nirD*, which encode the large and small subunits, respectively, of the nitrite reductase complex ($NirDB_2$); *hybO*, which encodes the small subunit of hydrogenase 2 (HybABOC); and *nrfA*, which is the structural gene for cytochrome c_{552} and a component of the formate-dependent nitrite reductase complex (NrfDCBA).

A second group of genes falls under protein maturation and modification, all of which—*hypA*, *hypB*,

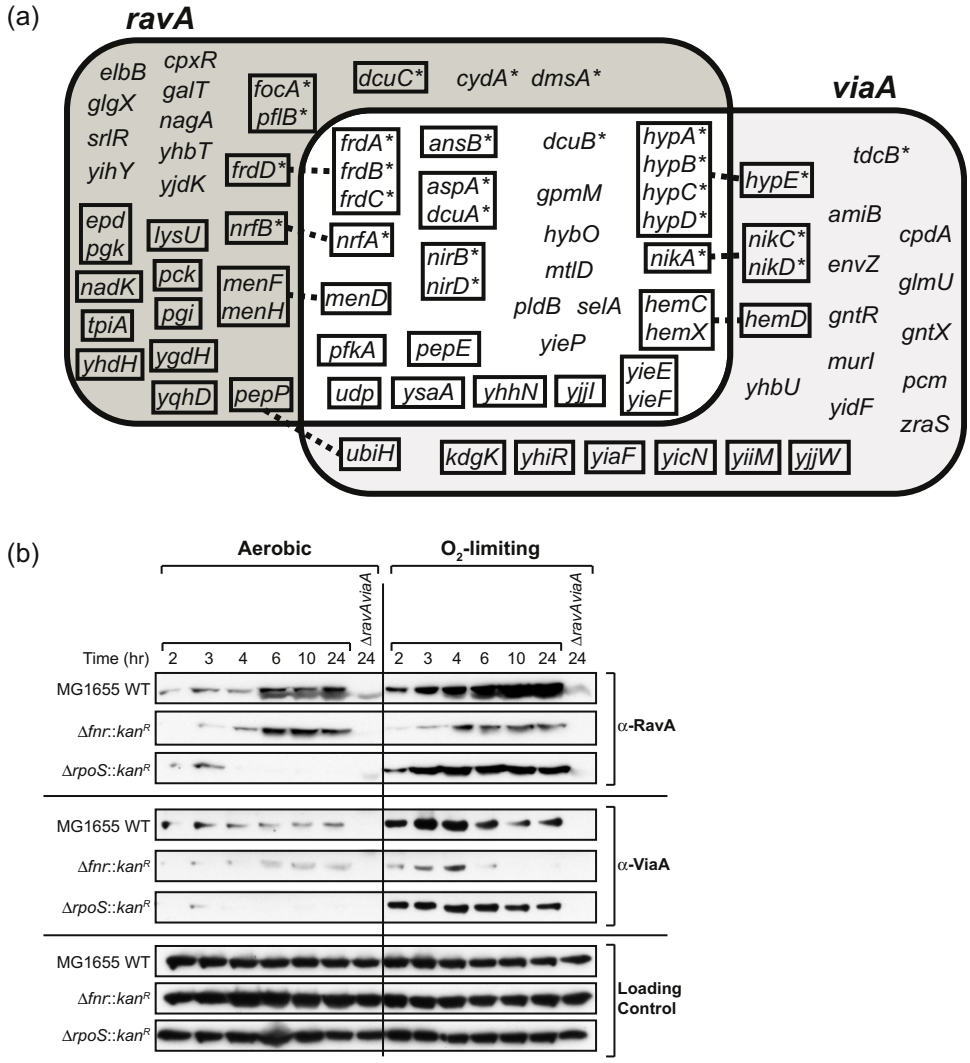

Fig. 1. Co-expression profiles and expression analysis for RavA and ViaA. (a) Shown are genes that have similar expression profiles as *ravA* and *viaA*. Single or multiple genes enclosed in rectangular boxes denote the constituents of monocistronic (only one gene included in its own box) or polycistronic operons (multiple genes in one box), respectively. Genes from the same polycistronic operon that are classified to a different co-expression category are linked with broken lines. All genes that are under the control of the transcriptional regulator Fnr are denoted with an asterisk (*). (b) Western blots of RavA and ViaA for aerobically grown cells (shown on the left) and cells grown under oxygen limitation (shown on the right). All strains were grown in LB media. The time points at which cells were harvested are as indicated at the top. The *ΔravAviaA* cells harvested after 24 h of growth were used to provide a reference for expressed RavA and ViaA. A cross-reacting band in the α-ViaA blots (at 70-kDa) that remains consistent at all the time points was used as the loading control.

hypC, and *hypD*—are involved in the insertion of Ni^{2+} ion for the maturation of the membrane-bound hydrogenase 3 (HycDCFGBE) and, thus, are also associated with anaerobiosis. Hydrogenase 3 works in conjunction with formate dehydrogenase H in both mixed acid fermentation and anaerobic respiration. Other genes that co-express with both *ravA* and *viaA* participate in various metabolic pathways (*gpmM*, *mtlD*, *pfkA*, *ansB*, *aspA*, *selA*, *pepE*, *pldB*, and *udp*), biosynthesis of cofactors and prosthetic groups (*hemC*, *hemX*, and *menD*), and transport of metabolites across the cell membrane (*dcuA*, *dcuB*, and *nikA*).

Importantly, 14 out of the 32 genes that co-express with *ravA* and *viaA* are inducible by the transcriptional regulator Fnr (marked with * in Fig. 1a). In *E. coli*, Fnr regulates the expression of a large number of genes during the transition from aerobiosis to anaerobiosis [28,29]. The co-expression of genes under Fnr control suggested that Fnr was also likely to regulate the expression of both *ravA* and *viaA*.

Table 1. Pearson correlation scores for *ravA*- and *viaA*-co-expressing genes and their functional annotations

Category I: Genes co-expressing with both *ravA* and *viaA*

Gene Name	b Number	Description	Correlation with *ravA*	Correlation with *viaA*
ansB	b2957	Asn metabolism	0.65051	0.60753
aspA	b4139	Asp metabolism	0.54194	0.57059
dcuA	b4138	C4-dicarboxylate transport	0.66535	0.54888
dcuB	b4123	C4-dicarboxylate transport	0.56817	0.51744
frdA	b4154	Anaerobic respiration; fermentation	0.69038	0.63405
frdB	b4153	Anaerobic respiration; fermentation	0.64379	0.60204
frdC	b4152	Anaerobic respiration; fermentation	0.61917	0.59640
gpmM	b3612	Glycolysis	0.59776	0.52958
hemC	b3805	Hem biosynthesis	0.51487	0.50138
hemX	b3803	Porphyrin biosynthesis	0.52810	0.54115
hybO	b2997	Anaerobic respiration	0.62005	0.58672
hypA	b2726	Protein modification; anaerobic respiration	0.64622	0.59540
hypB	b2727	Protein maturation	0.69607	0.62498
hypC	b2728	Protein maturation; anaerobic respiration	0.67458	0.63329
hypD	b2729	Protein modification; anaerobic respiration	0.65885	0.59676
menD	b2264	Menaquinone biosynthesis	0.54297	0.50761
mtlD	b3600	Carbohydrate catabolism	0.50802	0.56832
nikA	b3476	Ni^{2+} transport	0.54464	0.55937
nirB	b3365	Anaerobic respiration; nitrate assimilation	0.57724	0.51632
nirD	b3366	Anaerobic respiration; nitrate assimilation	0.53498	0.51578
nrfA	b4070	Anaerobic respiration	0.53363	0.51896
pepE	b4021	Glycopeptide catabolism	0.65684	0.56658
pfkA	b3916	Glycolysis	0.56294	0.51026
pldB	b3825	Lipid biosynthesis	0.52289	0.59484
selA	b3591	Selenocysteine incorporation	0.69996	0.62336
udp	b3831	Nucleoside metabolism	0.50767	0.53799
yhhN	b3468		0.54876	0.54350
yieE	b3712		0.58220	0.53172
yieF	b3713	Xenobiotic metabolism	0.55289	0.55248
yieP	b3755	Transcription regulation	0.59788	0.57585
yjjI	b4380		0.70975	0.69532
ysaA	b3573	Electron transport chain	0.61717	0.56855

Category II: Genes co-expressing with *ravA* only

Gene Name	b Number	Description	Correlation with *ravA*
cpxR	b3912	DNA-binding response regulator in two-component regulatory system with CpxA	0.56566
cydA	b0733	Cytochrome *d* terminal oxidase, subunit I	0.51738
dcuC	b0621	Anaerobic C4-dicarboxylate transport	0.52104
dmsA	b0894	Dimethyl sulfoxide reductase, anaerobic, subunit A	0.55480
elbB	b3209	Isoprenoid biosynthesis protein with amidotransferase-like domain	0.50812
epd	b2927	D-erythrose 4-phosphate dehydrogenase	0.50287
focA	b0904	Formate transporter	0.52822
frdD	b4151	Fumarate reductase (anaerobic), membrane anchor subunit	0.50535
galT	b0758	Galactose-1-phosphate uridylyltransferase	0.50055
glgX	b3431	Glycogen debranching enzyme	0.52472
lysU	b4129	Lysine tRNA synthetase, inducible	0.53954
menF	b2265	Isochorismate synthase 2	0.52301
nadK	b2615	NAD kinase	0.54078
nagA	b0677	*N*-acetylglucosamine-6-phosphate deacetylase	0.55783
nrfB	b4071	Nitrite reductase, formate-dependent, penta-heme cytochrome *c*	0.51511
pck	b3403	Phosphoenolpyruvate carboxykinase	0.50262
pepP	b2908	Proline aminopeptidase P II	0.51160
pflB	b0903	Pyruvate formate lyase I (inactive)	0.52252
pgi	b4025	Glucosephosphate isomerase	0.53519
pgk	b2926	Phosphoglycerate kinase	0.53232
srlR	b2707	GutR glucitol repressor	0.58033
tpiA	b3919	Triosephosphate isomerase	0.57139
viaA	b3745	VWA-containing protein associated with RavA	0.84586
yfbB	b2263	(1R,6R)-2-succinyl-6-hydroxy-2,4-cyclohexadiene-1-carboxylate synthase	0.50662
ygdH	b2795	Hypothetical protein	0.55430
yhbT	b3157	Predicted lipid carrier protein	0.52801
yhdH	b3253	Predicted oxidoreductase, Zn-dependent, and NAD(P)-binding	0.54479
yihY	b3886	Predicted inner membrane protein	0.53130
yjdK	b4128	Hypothetical protein	0.56851
yqhD	b3011	Alcohol dehydrogenase, NAD(P)-dependent	0.55211

Table 1 (*continued*)

Category III: Genes co-expressing with *viaA* only			
Gene Name	b Number	Description	Correlation with *viaA*
amiB	b4169	*N*-acetylmuramoyl-l-alanine amidase II	0.52138
cpdA	b3032	Cyclic 3′,5′-adenosine monophosphate phosphodiesterase	0.53408
envZ	b3404	Sensory histidine kinase in two-component regulatory system with OmpR	0.53976
glmU	b3730	Fused *N*-acetyl glucosamine-1-phosphate uridyltransferase and glucosamine-1-phosphate acetyl transferase	0.52324
gntR	b3438	DNA-binding transcriptional repressor	0.57190
gntX	b3413	Gluconate periplasmic binding protein with phosphoribosyltransferase domain, GNT I system	0.50584
hemD	b3804	Uroporphyrinogen III synthase	0.50487
hypE	b2730	Carbamoyl phosphate phosphatase, hydrogenase 3 maturation protein	0.51627
kdgK	b3526	2-keto-3-deoxygluconokinase	0.54256
murI	b3967	Glutamate racemase	0.51627
nikC	b3478	Nickel transporter subunit	0.52011
nikD	b3479	Nickel transporter subunit	0.50367
pcm	b2743	L-isoaspartate protein carboxylmethyltransferase type II	0.53129
ravA	b3746	MoxR AAA+ ATPase interacting with LdcI	0.84586
tdcB	b3117	Catabolic threonine dehydratase, PLP-dependent	0.51152
ubiH	b2907	2-octaprenyl-6-methoxyphenol hydroxylase, FAD/NAD(P)-binding	0.51134
yhbU	b3158	Predicted peptidase, collagenase-like	0.54514
yhiR	b3499	Protein utilizing DNA as a carbon source	0.53345
yiaF	b3554	Hypothetical protein	0.52386
yicN	b3663	Hypothetical protein	0.62638
yidF	b3674	Predicted DNA-binding transcriptional regulator	0.55130
yiiM	b3910	Protein involved in base analog detoxification	0.53678
yjjW	b4379	Predicted pyruvate formate lyase activating enzyme	0.54970
zraS	b4003	Sensory histidine kinase in two-component regulatory system with ZraR	0.54079

The table contains a list of genes that meet the stringent cutoff (correlation score ≥ 0.5) and are considered to co-express with *ravA* and/or *viaA*. The Pearson correlation scores corresponding to each of these genes are provided on the right. The b numbers and functional descriptions (if available) are also provided as shown. The genes are divided into three categories, depending on whether they co-express with both *ravA* and *viaA* (Category I), with *ravA* only (Category II), or with *viaA* only (Category III). A Venn diagram of the data is given in Fig. 1a.

Fnr enhances the expression of RavA and ViaA during oxygen-limiting conditions

To determine whether the expression of RavA and ViaA was indeed regulated by Fnr, we have grown wild-type (WT) along with the null mutants *Δfnr*::*kan*^{R} and *ΔrpoS*::*kan*^{R} in liquid media under aerobic or oxygen-limiting conditions. Cell growth was monitored by measuring OD_{600} at specific time points. When cells were grown aerobically, all three strains shared almost identical growth profiles (Fig. S1). On the other hand, during oxygen-limiting growth, *Δfnr*::*kan*^{R} exhibited a minor growth lag from early log to late log phase, and both *Δfnr*::*kan*^{R} and *ΔrpoS*::*kan*^{R} had only a slightly lower cell count per unit volume compared to WT upon reaching stationary phase (Fig. S1). These relatively small differences in growth between WT and the two mutants helped minimize changes in experimental protocol, which were made to accommodate their different growth profiles.

The expression levels of RavA and ViaA in each strain were then analyzed by Western blotting. Under aerobic condition, WT cells displayed the expected RavA expression profile as reported previously [6], with minimal expression during log phase that increases to optimum at stationary phase (Fig. 1b). Interestingly, under oxygen-limiting condition, RavA expression was significantly enhanced in WT cells at all growth phases, which indicates that oxygen starvation is likely an important inducer of RavA protein expression. Importantly, unlike in the WT cell line, the expression of RavA in *Δfnr*::*kan*^{R} cells did not increase during oxygen-limiting growth. Thus, Fnr was deemed necessary for the enhanced expression of RavA when oxygen is limiting. Furthermore, as previously reported in aerobically grown *ΔrpoS*::*kan*^{R} cells, the expression of RavA was severely compromised due to the loss of σ^S [6]. In contrast, under oxygen-limiting condition, the expression of RavA in *ΔrpoS*::*kan*^{R} closely resembles that of WT, although the further increase in RavA levels after 6 h observed in WT was not observed in *ΔrpoS*::*kan*^{R} (Fig. 1b). This strongly supports the conclusion that the expression of RavA during oxygen starvation is largely dependent on Fnr and not σ^S, but σ^S might have some role at later time points.

Like RavA, the expression of ViaA shows a similar dependence on Fnr in cells during oxygen starvation. In WT cells, ViaA expression was significantly enhanced, and the deletion of σ^S did not affect this enhancement; however, in the absence of Fnr, no such

enhancement was observed (Fig. 1b). It is interesting to note that ViaA expression during oxygen-limiting growth was higher in log phase compared to stationary phase—the reverse of RavA. This was most apparent in WT and *Δfnr*::*kan*^{R} cells (Fig. 1b). In contrast, ViaA expression was largely unchanged in *ΔrpoS*::*kan*^{R} cells during oxygen starvation from log phase to stationary phase (Fig. 1b). Since both *ravA* and *viaA* are on the same operon [6] and there is no recognizable promoter upstream of *viaA*, the difference in the expression profiles of RavA and ViaA likely reflects the presence of additional regulatory elements affecting either mRNA or protein levels that are dependent on σ^S.

Overall, our results clearly illustrate that, under oxygen-limiting conditions, Fnr functionally replaces σ^S and becomes the primary regulator for the expression of both RavA and ViaA, which makes both the *ravA* and *viaA* genes novel constituents of the Fnr regulon. However, σ^S continues to play a role in RavA and ViaA expression under these conditions.

Identification of potential Fnr binding sites in the native promoter region of *ravAviaA*

The Fnr-induced expression of RavA and ViaA cells during oxygen-limiting growth indicates the existence of regulatory elements in the *ravAviaA* promoter region for Fnr binding. Identification of such elements would further validate the results of Fig. 1.

Using knowledge-based sequence motif recognition software such as Virtual Footprint [30], SCOPE [31], and PromoScan [32], our initial analysis of the genomic sequence of this region to identify the potential binding sites of various transcriptional regulators revealed two potential Fnr binding sites: one centered at −72.5 (**TT**A**A**CCTGGC**TCAA**; bolded bases represent perfect matches to the Fnr consensus sequence) and another one located further upstream at −188.5 (**TTG**C**T**TATT**ATCA**G;Fig. 2a and b). Both sites are similar to the Fnr consensus sequence TTGATnnnnATCAA (n represents any base) [33], but they lack the characteristic palindromic sequences that flank the two ends.

To further examine these two potential binding sites for Fnr, we synthesized three linear DNA substrates of the same length but that encompass different parts of the *ravAviaA* promoter region (R-1, R-2, and R-3; Fig. 2c) by PCR for use in electromobility shift assay (EMSA) assays with Fnr_{D154A}. The Fnr_{D154A} mutant, which has the same affinity and specificity for the Fnr consensus sequence as its WT counterpart [34], was used so that the EMSA experiments could be performed under aerobic conditions. As shown in Fig. 2d, the inclusion of Fnr_{D154A} in the sample induced significant band shifts for DNA substrates R-1 (which has both the −72.5 and −188.5 Fnr binding sites) and R-2 (which retains only the −72.5 site). In contrast, band shift was reduced for substrate R-3, which lacks both supposed Fnr binding sites. As both R-1 and R-2 displayed very similar band shifts in the presence of Fnr_{D154A}, the −188.5 site did not appear to be necessary for binding. In other words, the interaction between Fnr_{D154A} and the *ravAviaA* promoter appears to be largely mediated through the −72.5 site.

To provide additional proof that the interaction between Fnr_{D154A} and the DNA substrates R-1 and R-2 was specific, we repeated EMSA using the following substrates: F-1 as negative control, and H-1, H-2, and H-3 as positive controls (Fig. 2e–g). Substrate F-1 encompasses the entire *fepDGC* promoter region, which carries four binding sites for the Fe^{2+}-sensing Fur [35–37] but none for Fnr. Substrate H-1 encompasses the *hypBCDE* promoter region that is internal to the *hypA* gene. It contains two Fnr binding sites—one centered at −43.5 (**TTGAT**CTGGT**T**TGC; bolded bases represent perfect matches to the Fnr consensus sequence) and the other one further upstream at −149.5 (**TTGAT**CGAACAGC**A**) [38]. Following the same scheme used in examining the Fnr binding sites from the *ravAviaA* promoter, substrates H-2 (only the −43.5 site is retained) and H-3 (all Fnr binding sites removed) were also synthesized. As shown in Fig. 2g, Fnr_{D154A} did not interact with either F-1 or H-3, as neither substrate carries Fnr binding sites. On the other hand, H-1 contains both Fnr binding sites, and it interacted strongly with Fnr_{D154A}, resulting in a significant band shift. For substrate H-2, removal of the upstream −149.5 Fnr binding site severely reduced its interaction with Fnr_{D154A}. Thus, the binding of Fnr_{D154A} to substrates R-1, R-2, and H-1 was indeed specific.

With binding of Fnr to the *ravA* promoter established, a β-galactosidase transcriptional reporter-based colorimetric assay was used to evaluate each of the two identified Fnr binding sites in regulating the expression of RavA and ViaA. The *lacZ* gene that encodes β-galactosidase was placed downstream of the native *ravA* (i.e., *ravAviaA*) promoter to create pP_{ravA}-*lacZ*. Two additional plasmids were also used for determining the influence of each of the two Fnr binding sites: pP_{ravAm1}-*lacZ*, which has the −72.5 Fnr site replaced with a 14-bp non-native sequence composed of a NheI restriction site flanked by random bases on both ends; and pP_{ravAm2}-*lacZ*, which has the −188.5 Fnr site mutated, while its −72.5 site retains its native sequence (Fig. 2h; see Materials and Methods for details). *E. coli* EDCM 367 cells (MG1655 *lacZ*$^-$, *lacY*$^-$) transformed with these constructs were grown under oxygen-limiting condition, and the cell lysates generated from them were subjected to the Miller assay to measure the β-galactosidase activity. A *lacZ* construct lacking the *ravA* promoter (pΔP-*lacZ*) was used to observe background color development unrelated to β-galactosidase production. An EDCM 367 Δ*fnr* strain transformed with pP_{ravA}-*lacZ* was used as a control for Fnr-independent *lacZ* transcription

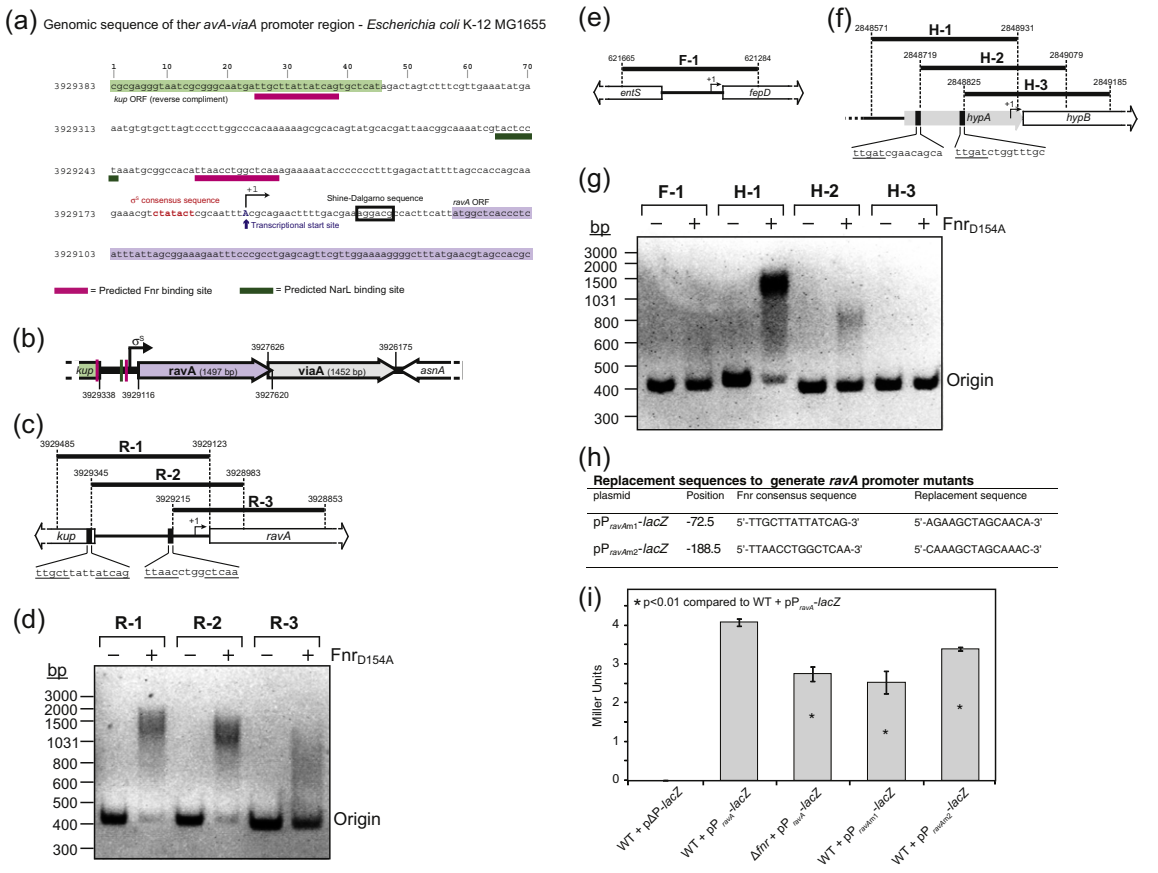

Fig. 2. The *ravAviaA* promoter region and its regulation by Fnr. (a) Sequence for the *ravA* and nearby *kup* (encodes the K^+ transporter; shown here in reverse complement) ORFs are colored in purple and green, respectively. The σ^S consensus sequence in red [64], transcription start site in blue [65], and the Shine–Dalgarno sequence in black box are indicated as shown. The potential Fnr binding sites are underlined in pink, and a putative 7-nt stretch of sequence matching the NarL consensus site is underlined in green. The genomic coordinates are given to the left of each line. (b) Genetic layout for the *ravA-viaA* and *kup* genes is represented, highlighting the position of the σ^S consensus sequence, the two putative Fnr binding sites (pink bars), and a site matching the NarL consensus sequence (green bar). (c, e, and f) Schematic representations of the DNA substrates R-1, R-2, and R-3 for the (c) *ravAviaA* promoter region, (e) F-1 for the *fepD* promoter region, and (f) H-1, H-2, and H-3 for the *hypBCDE* promoter region. Both putative and confirmed binding sites for Fnr are indicated with black boxes as illustrated, and their DNA sequences are shown below. Bases that are underlined represent the half-sites (both putative and confirmed) that are crucial for Fnr binding [33,38]. The genomic region covered by each DNA substrate is indicated at both ends with the corresponding *E. coli* K-12 genome coordinates. Bent arrows represent the transcriptional start sites (+1). (d and g) EMSA results using substrates (d) R-1, R-2, and R-3, and (g) F-1, H-1, H-2, and H-3. The absence (–) and presence (+) of Fnr_{D154A} in the reaction mixture are as indicated at the top. The origins of all DNA substrates used are as shown. The MWs of the DNA markers used are shown on the left of the gel. (h) The mutations made at the Fnr binding sites within the *ravA* promoter region are listed. (i) A graph representing the β-galactosidase activity levels in cells grown under oxygen limitation is shown when under the control of the indicated promoter region. Either EDCM 367 (WT) cells or the EDCM 367 Δ*fnr* (Δ*fnr*) strains were used. β-galactosidase expression, encoded by *lacZ*, was under the control of no promoter (pΔP-*lacZ*), *ravA* native promoter (pP_{ravA}-*lacZ*), or the RavA promoters mutated at either of two Fnr binding sites (pP_{ravAm1}-*lacZ* or pP_{ravAm2}-*lacZ*). *p*-values comparing the Δ*fnr* + pP_{ravA}-*lacZ*, WT + pP_{ravAm1}-*lacZ*, and WT + pP_{ravAm2}-*lacZ* with WT + pP_{ravA}-*lacZ* are indicated with * and noted at the top of the graph.

due to the activity of other unidentified transcriptional regulators on the native *ravA* promoter. As shown in Fig. 2i, the presence of Fnr in the cell contributes to about 50% increase in β-galactosidase activity and correspondingly in *lacZ* expression while under the control of the native *ravA* promoter. This difference accounts for the expression of *lacZ* that is Fnr dependent and agrees with our RavA-ViaA expression profile during oxygen-limiting growth as discussed above (Fig. 1b). Importantly, abolishment of

the −72.5 Fnr recognition sequence in pP_{ravAm1}-*lacZ* led to a complete loss of the Fnr-dependent *lacZ* expression despite the presence of Fnr and resulted in a β-galactosidase activity, which resembles that obtained from the EDCM 367 Δ*fnr* + pP_{ravA}-*lacZ* control. In contrast, abolishment of the −188.5 site resulted in only a mild reduction in Fnr-dependent *lacZ* expression, which remained ~24% higher than that of EDCM 367 Δ*fnr* + pP_{ravA}-*lacZ*. Thus, the −72.5 Fnr site is revealed to be the primary site for the Fnr-dependent induction of the *ravA* promoter, while the −188.5 site plays a secondary role. This is consistent with our EMSA result, which shows that the binding of Fnr_{D154A} to the *ravA* promoter occurs primarily on the −72.5 Fnr site (Fig. 2d).

In the time course analysis for RavA levels (Fig. 1b), some amount of RavA was observed to be present in the absence of Fnr. Similarly, a basal level of β-galactosidase activity was observed in the Fnr knockout (KO) strains (Fig. 2i). It is conceivable, not accounting for post-translational regulation of the protein levels, that other transcription factors may play a part in the expression and regulation of the *ravAviaA* operon. Along with the Fnr binding sites mentioned above, a 7-nt sequence-centered 96 nt upstream of the RavA open reading frame (ORF) was found to match the consensus sequence for the NarL transcription factor (Fig. 2a) [39]. However, the mutation of this proposed recognition sequence had no effect on β-galactosidase activity (not shown).

ViaA physically interacts with uncomplexed FrdA in oxygen-starved cells and the interaction is modulated by RavA

Next, given that RavA and ViaA are induced primarily by Fnr under oxygen-limiting conditions (Figs. 1 and 2), we carried out experiments to identify the physical interactors of RavA and ViaA under these conditions, particularly those that are also upregulated by Fnr. To this end, strains that express endogenous C-terminally sequential peptide affinity (SPA)-tagged proteins were used [40], followed by the detection of RavA and/or ViaA bound to the isolated protein complexes through Western blotting. The SPA tag is a dual-affinity tag consisting of 3xFLAG and a calmodulin-binding peptide motif separated by a cleavage site for tobacco etch virus (TEV) protease. The choices of proteins to be tagged were based on the results of our co-expression profiling for *ravA* and *viaA* and on the several high-throughput studies that we previously carried out [9,17].

As shown in Fig. 3a, among the 22 proteins that were successfully SPA-tagged, ViaA [untagged; molecular weight (MW) = 56 kDa] was observed to interact strongly with SPA-tagged FrdA. FrdA is

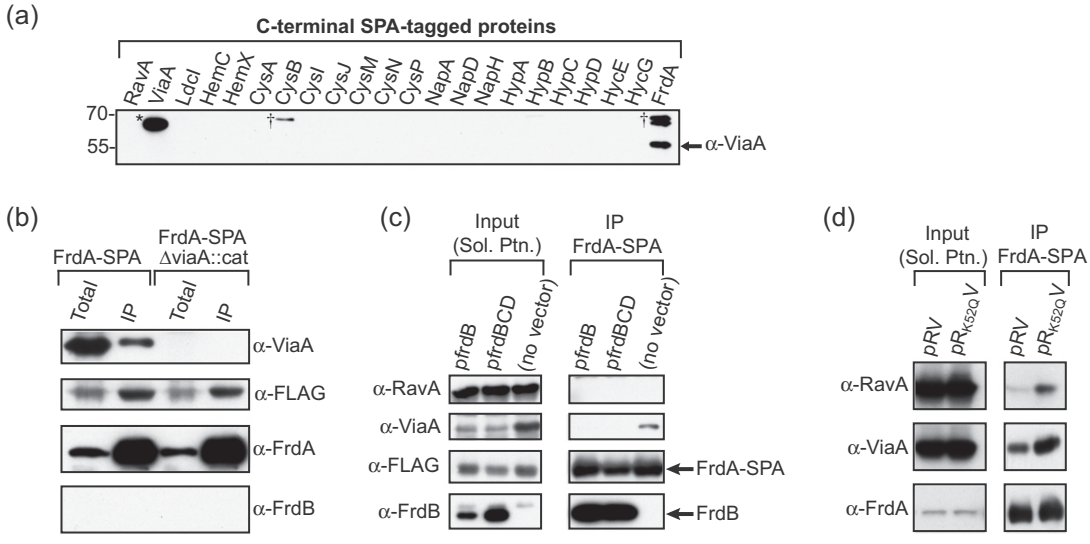

Fig. 3. The interaction of ViaA with FrdA. (a) Initial screen to identify physical interactors of ViaA in DY330 cells grown under oxygen limitation in LB. SPA tag was fused to the endogenous genes. The identities of bait proteins are as given at the top. "*" denotes ViaA-SPA. "†" denotes cross-reacting bands in the α-ViaA blot. The ViaA band is indicated by an arrow. (b) Confirmation of the interaction between ViaA and FrdA-SPA. Note that FrdB expression was abolished due to the introduction of the SPA tag. All cells were grown under oxygen limitation in LB. Identities of the strains are given at the top. Total refers to soluble proteins from total cell lysate; IP refers to proteins found in the immunoprecipitation of FrdA-SPA. (c) Western blots of total RavA, ViaA, FrdA-SPA, and FrdB in DY330 FrdA-SPA strain grown under oxygen limitation and after the immunoprecipitation of FrdA-SPA. Sol. Ptn. = soluble proteins; IP = immunoprecipitation. (d) Western blots for total RavA, ViaA, and FrdA in DY330 FrdA-SPA strain transformed with pRV or $pR_{K52Q}V$ grown under oxygen limitation and after the immunoprecipitation of FrdA-SPA.

the FAD-binding component of the Frd complex (FrdABCD) that is involved in anaerobic respiration [18]. ViaA was not observed when FrdA-SPA pull-down was repeated in Δ*viaA* cells (Fig. 3b), which confirms the validity of the observed ViaA–FrdA interaction. None of the SPA-tagged proteins interacted with RavA, with the only exception being LdcI-SPA (data not shown), which agrees with our previous report [6]. In addition, we had previously shown that RavA only interacts weakly or transiently with ViaA [6], and accordingly, no ViaA was brought down with RavA-SPA and vice versa (data not shown).

In the FrdA-SPA strain, the expression of the Fe–S cluster-containing subunit of Frd, FrdB, was compromised due to the introduction of the SPA tag (Fig. 3b). Similarly, given that both *frdC* and *frdD* are located downstream of *frdB*, expressions of FrdC and FrdD were presumed to be compromised as well; however, antibodies against these two proteins were not available for us to test this. Hence, the interaction between ViaA and FrdA-SPA does not require endogenous FrdBCD, as ViaA seems to bind free FrdA.

To further investigate this observation, we transformed the FrdA-SPA strain with plasmids that overexpress either the FrdB alone or the FrdBCD subunits of the Frd complex, and the immunoprecipitation experiments were repeated. No interaction was observed between FrdA and ViaA in the presence of FrdB or FrdBCD (Fig. 3c; IP). We interpret these results to mean that ViaA binds free FrdA and not FrdA in an FrdAB or FrdABCD complex.

In light of the interaction of FrdA-SPA with ViaA, the potential role of RavA in modulating this interaction was also investigated. The immunoprecipitation experiments were repeated for FrdA-SPA strain transformed with the plasmids pRV or $pR_{K52Q}V$. The pRV plasmid expresses WT ViaA and RavA. The $pR_{K52Q}V$ plasmid expresses WT ViaA and a mutant RavA in which the lysine residue of the Walker A motif is mutated to glutamine, rendering the protein ATPase inactive. As shown in Fig. 3d, protein levels were the same (input); however, more ViaA and RavA bound FrdA-SPA in the presence of ATPase-deficient RavA. We speculate that RavA ATPase activity disrupts or weakens the ViaA–FrdA interaction.

ViaA associates with RavA through its N-terminal domain and with FrdA through its C-terminal VWA domain

The pull-downs in Fig. 3 point toward ViaA as the common partner binding to FrdA and RavA in a potential tertiary complex since RavA alone was not pulled down by FrdA. To verify direct interactions among FrdA and ViaA and to identify the role of ViaA domains in mediating the transient RavA–ViaA–FrdA complex formation, we performed co-immunoprecipitation experiments with purified proteins. A schematic of the ViaA domain arrangement is shown in Fig. 4a. This was obtained based on the sequence alignment of ViaA from several bacterial species and on partial protease digestion (not shown). The VWA domain of ViaA is at the C terminus [6]. We named this domain CTV for C-terminal domain of ViaA. The N-terminal domain of ViaA (NTV) appears to be novel with little sequence similarity to any characterized protein. The purified isolated NTV domain was stable (see below), but CTV was highly insoluble and was fused to a NusA tag to stabilize it (see Materials and Methods).

Pull-down experiments were carried out with the FrdA-SPA construct used as the bait. Figure 4b depicts the results whereby purified RavA, ViaA, and its CTV and NTV domains were used as prey for the pull-downs either with FrdA-SPA bound to anti-FLAG M2-affinity beads or by using the beads without any bound protein. After washing, proteins were eluted using TEV protease. The protease cleaves the FLAG-tag moiety of the SPA tag fused to the C terminus of FrdA. In the instance where no protein was bound onto the beads, mock elutions were performed under the same conditions. No significant interaction was observed between RavA and FrdA, consistent with the results in Fig. 3a and d. On the other hand, ViaA eluted with FrdA, thus showing a direct interaction between the two proteins. More specifically, despite some basal level of association with the beads, an increase in NusA-CTV co-elution was seen in the presence of FrdA, while the NTV did not bind FrdA-SPA at all. Also, NusA alone did not bind FrdA. These pull-downs show that ViaA associates with FrdA through its VWA domain.

Based on the above results, since CTV in ViaA binds FrdA, we speculated that NTV in ViaA binds RavA. We initially biochemically characterized the NTV domain. Like ViaA, NTV (theoretical MW of 36 kDa) was found as a mainly monomeric protein by size-exclusion chromatography (SEC; Fig. 5a) and sedimentation equilibrium analytical ultracentrifugation (Fig. 5b). NTV was found to be enriched in α-helices (32%) and β-sheets (22%) at 20 °C as measured by circular dichroism (CD) spectroscopy (Fig. 5c) and to be highly stable with a T_m of 66.1 °C under the conditions tested (Fig. 5d). Next, we made use of our previous observation that RavA ATPase activity is enhanced by ViaA [6] to check for the potential interaction of NTV with RavA. RavA ATPase activity was tested in the presence of ViaA and its different domain constructs. The activity of RavA (measured at 0.5 μM protomer concentration) was increased to similar levels by equimolar concentration of full-length ViaA protein or NTV (Fig. 5e). The presence of NusA-CTV or NusA had no significant effect on RavA ATPase (Fig. 5e). Hence, the results indicate that ViaA associates with RavA through its NTV segment. Furthermore, by measuring the ATPase activity enhancement of RavA at different

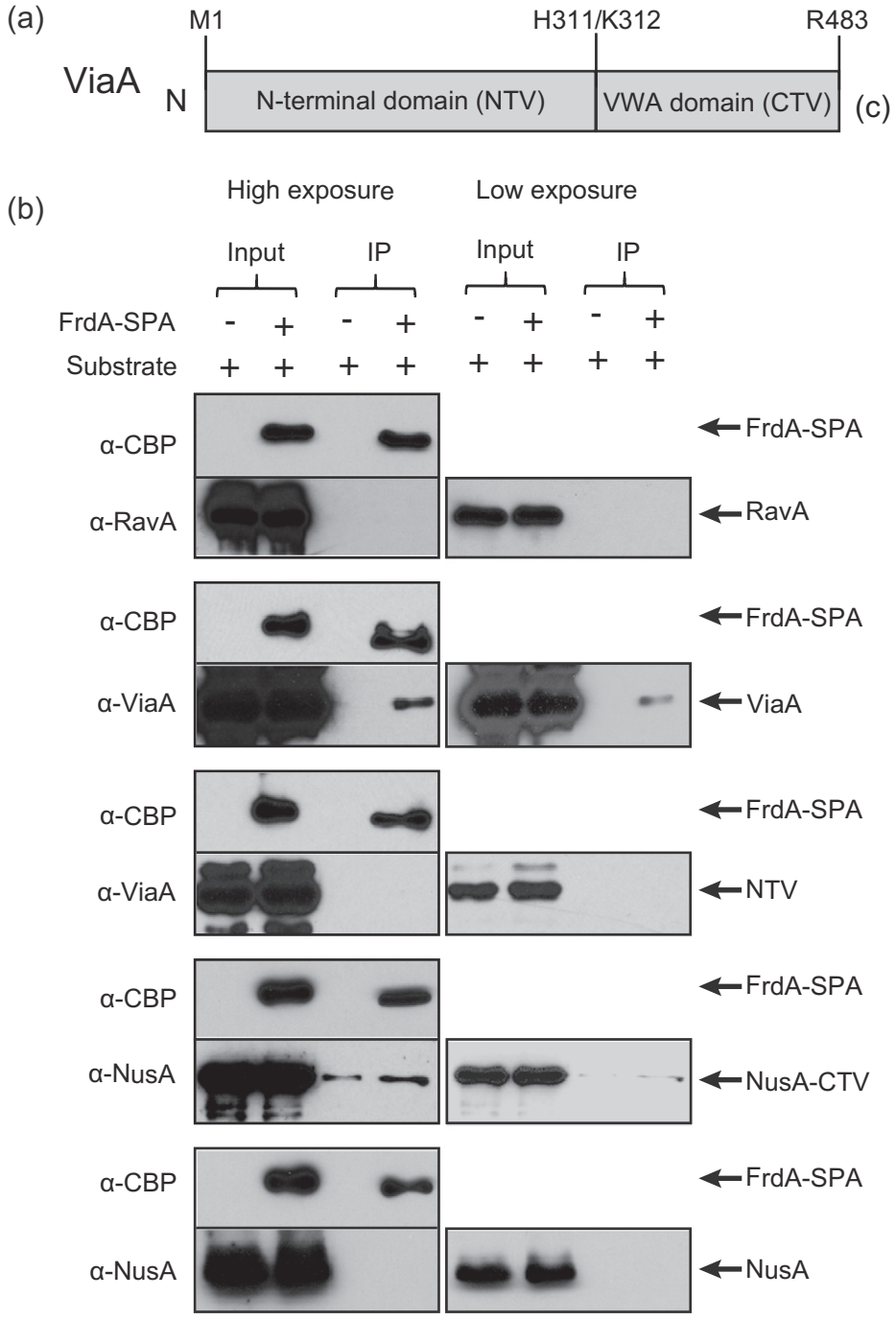

Fig. 4. Pull-down assays mapping the interaction of ViaA domains with RavA and FrdA. (a) A schematic of the ViaA protein showing the domain boundaries of NTV (residues 1–311) and CTV (312–483). (b) Western blots are shown for the immunoprecipitation performed either with FrdA-SPA bound onto FLAG-affinity beads or with empty beads. Purified RavA, ViaA, NTV, NusA-CTV, or NusA proteins were added to the beads as indicated. The antibody used for detection is noted on the left with the respective detected protein indicated on the right. High and low exposure blots are shown for clarity.

concentrations of the full-length ViaA protein or the NTV domain (Fig. 5f), we obtained apparent dissociation constants of 0.15 μM and 0.55 μM for the ViaA–RavA and NTV–RavA associations, respectively.

Taken together, the results of Figs. 4 and 5 show that ViaA can be considered as an adaptor protein that interacts with RavA via its NTV and with FrdA via its CTV.

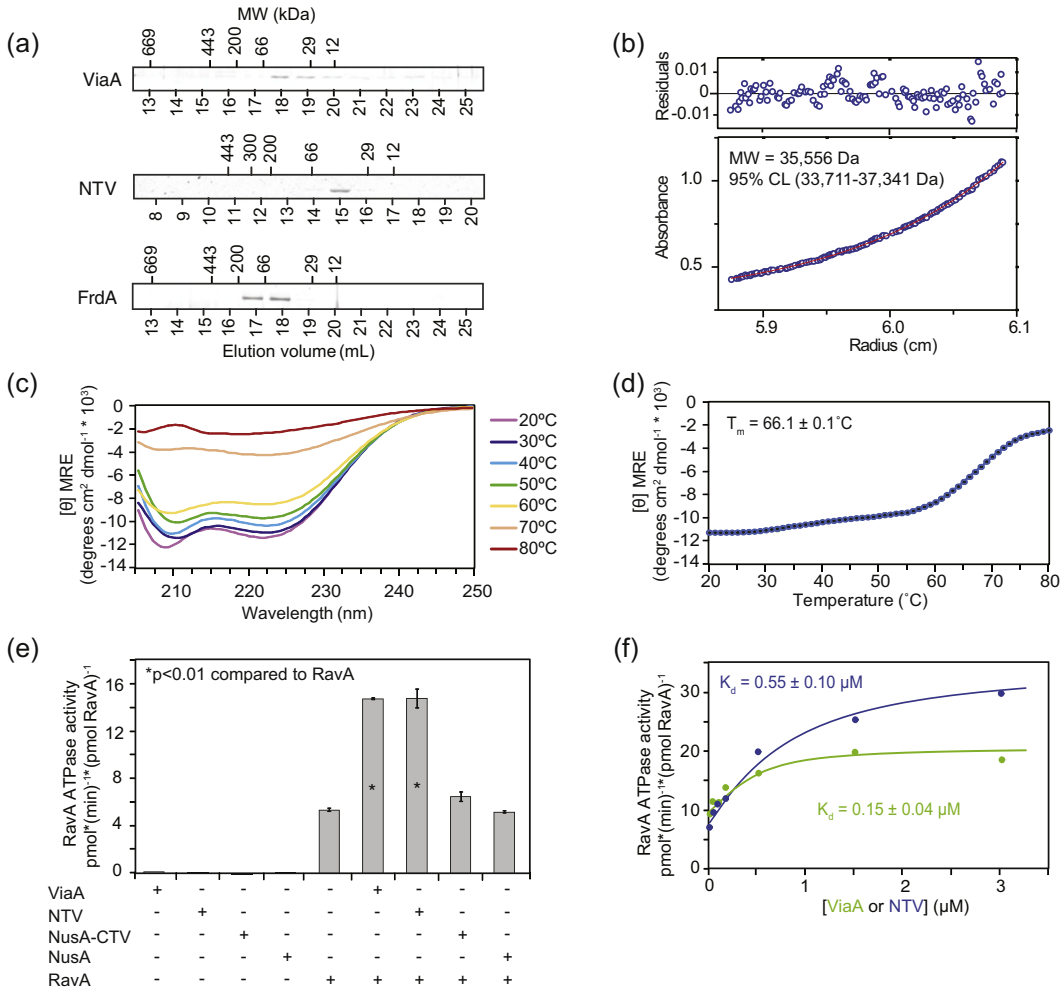

Fig. 5. Characterizing the interaction of NTV with RavA. (a) SEC of the ViaA and FrdA proteins on Superose 6 column and of NTV on Superdex 200 column. MW markers are indicated on the top of each panel with the elution volumes noted on the bottom. (b) The lower panel shows the analytical ultracentrifugation sedimentation equilibrium data for NTV at 14 μM at 4 °C. The solid line is the theoretical fit to the data using a single-species function. The MW and the 95% confidence interval values are given. The upper panel displays residual deviations from the theoretical fit. (c) Shown are the CD wavelength scans for NTV as a function of temperature. (d) Thermal melt of NTV monitored by CD at 222 nm. The melting temperature (T_m) is given above the curve. (e) RavA (0.5 μM) ATPase activity rates in the presence of equimolar amounts of ViaA, NTV, NusA-CTV, or NusA proteins. A "*" indicates that the difference from the ATPase activity of RavA alone is significant, p-value <0.01. (f) Change in RavA ATPase activity as a function of ViaA (green) or NTV (blue) concentration. The data were fit to a single binding site model to obtain an apparent K_d. Data from one titration experiment are shown. The experiment was repeated three times to obtain the average K_d.

RavA-ViaA regulate the activity of the Frd complex in *E. coli*

Both the physical interaction between ViaA and FrdA-SPA and the antagonistic effect of RavA on the FrdA–ViaA interaction suggest that RavA-ViaA might functionally modulate the activity of the Frd complex. To test this possibility, we isolated inverted membrane vesicles from anaerobically grown MG1655 cells expressing different levels of RavA and/or ViaA. The isolated vesicles containing the Frd complex were then examined for differences in Frd activity *in vitro* by measuring the oxidation of benzyl viologen (BV) in the presence of fumarate (see Materials and Methods).

As shown in Fig. 6a, vesicles isolated from *ΔravAviaA* and *ΔravAviaA* + p11 (p11 is an empty vector) strains showed an increase greater than 43% in Frd activity compared to WT vesicles. In contrast, addition of RavA and ViaA (*ΔravAviaA* + pRV) resulted in the reduction of Frd activity to near WT levels. As a control, assay performed in the absence of fumarate or with vesicles from *ΔfrdA*::*kan*^{R} strain did not show any Frd activity, which highlights the

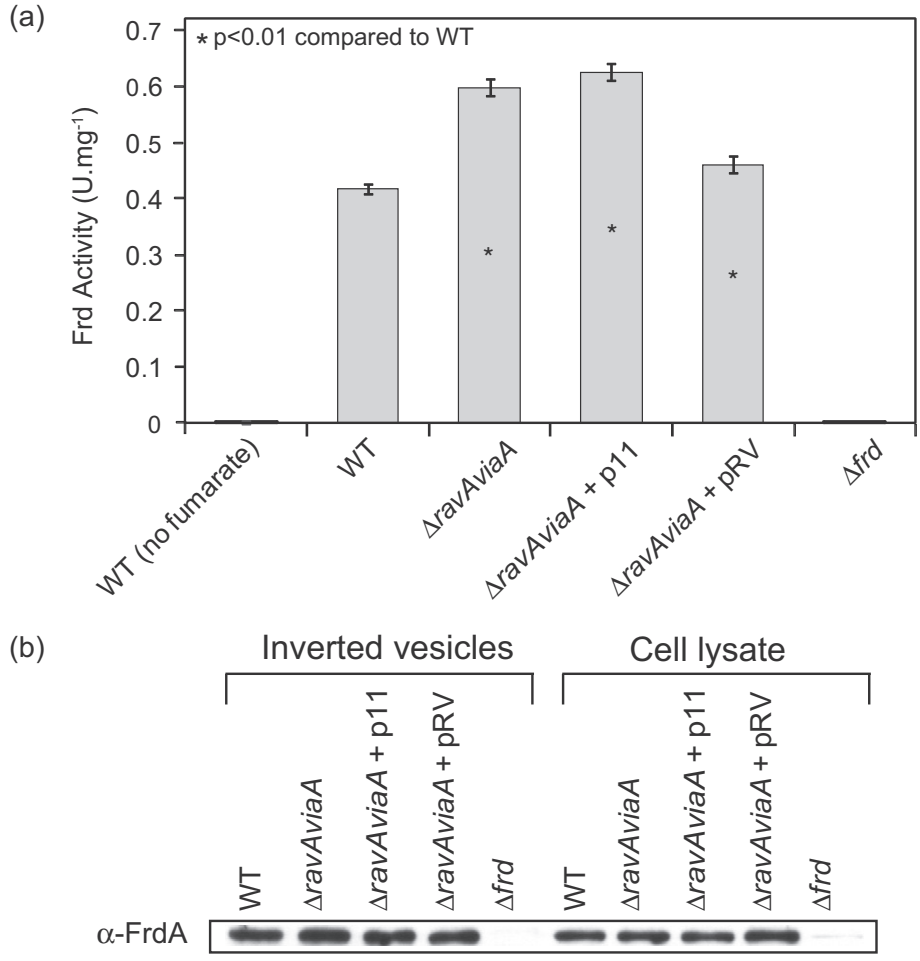

Fig. 6. RavA-ViaA modulate Frd activity in oxygen-starved *E. coli* MG1655. (A) BV assay on inverted membrane vesicles isolated from cells expressing different levels of RavA and ViaA. The strains used are identified below the graph. Three independent experiments were conducted for each strain. 1 U = 1 μmol BV oxidized per minute. *p*-values <0.01 were obtained when comparing the Δ*ravAviaA*, Δ*ravAviaA* + p11, and Δ*ravAviaA* + pRV Frd activities with WT activity. This is indicated with *. (B) Western blotting confirms that protein levels of FrdA remain unchanged upon changes in RavA and ViaA levels.

specificity of this assay in capturing only the activity of the Frd complex. Importantly, neither RavA nor ViaA had any observable effects on the expression levels of FrdA (and presumably FrdB, FrdC, and FrdD; Fig. 6b). Hence, RavA and ViaA play a role in mediating the rate of fumarate reduction by the Frd complex by possibly regulating its maturation and assembly.

Discussion

In this study, we elucidated a novel functional association of the MoxR protein RavA and its VWA partner, ViaA, from *E. coli* with the Frd complex during anaerobiosis. The interaction between the RavA-ViaA system and the Frd complex modulates the activity of the complex (Fig. 6). This association was revealed due to our observation that RavA and ViaA are overexpressed under oxygen-limiting conditions. Although other transcription factors may also be responsible, the expression of RavA-ViaA during oxygen starvation was found to be primarily inducible by the transcriptional regulator Fnr, which also regulates the expression of the Frd complex and other proteins involved in anaerobiosis [29,41]. Our finding of the regulation of the *ravAviaA* promoter by Fnr is consistent with a recent high-throughput study based on a ChIP-chip approach (combining chromatin immunoprecipitation with DNA microarray readout) [42].

Importantly, the role of σ^S in the induction of RavA-ViaA expression is significantly diminished and largely relinquished to Fnr during oxygen-limiting growth. This coincides with a previous report in which the expression of σ^S in *E. coli* MC4100 and MG1655

was shown to decrease during anaerobiosis [43]. Nevertheless, our data indicate that σ^S does have a role in modulating the expression of RavA and ViaA under oxygen-limiting conditions. Under these conditions, RavA expression is induced in log phase but then drastically further increases in stationary phase. However, ViaA expression peaks at log phase and then decreases in stationary phase (Fig. 1b). In the absence of σ^S, this biphasic opposing regulation of RavA and ViaA is not observed to a significant extent (Fig. 1b). Hence, σ^S differentially modulates the expression of ViaA and RavA under oxygen starvation. Under these conditions, σ^S might, for example, induce a protease that degrades ViaA but not RavA. Alternatively, given that *ravA-viaA* form an operon, σ^S might indirectly regulate the translation of the *ravA-viaA* mRNA.

In a previous report, we had shown that RavA and ViaA interact both physically and functionally with specific subunits of the Nuo complex [9]. RavA-ViaA interact primarily with the flavin mononucleotide-binding NuoF subunit under aerobic conditions and with the fused NuoCD subunit under anaerobic conditions [9]. Importantly, the Nuo complex is known to be involved in both the aerobic and the anaerobic respiration of *E. coli* [14,15]. It has also been shown that the coupling between the Nuo complex and the Frd complex is important for the electron transfer from NADH to fumarate during anaerobic respiration of *E. coli* [16]. Taken together, our results support a potential regulatory role of RavA-ViaA in the anaerobic utilization of fumarate via its interaction with both the Nuo and Frd complexes.

Our current working model of the effect of RavA-ViaA on the assembly of the Frd complex is depicted in Fig. 7. We had shown previously that ViaA tends to associate with the bacterial inner membranes [9]. Hence, we speculate that an initial interaction occurs between the flavoenzymatic FrdA subunit of the Frd complex and ViaA at the inner membranes. This occurs with free FrdA in the absence of FrdB, as the presence of FrdB precludes this association. Although RavA was not observed to directly bind FrdA, a tertiary complex of RavA–ViaA–FrdA was clearly seen when the ATPase-deficient mutant of RavA was used (Fig. 3d). ViaA acts as an adaptor in this complex by using its N-terminal domain to bind to RavA and its C-terminal VWA domain to bind FrdA (Figs. 4 and 5). The ATPase activity of RavA seems to facilitate the disassembly of the ViaA–FrdA association (Fig. 3d). If FrdB is then available, the free FrdA can associate with FrdB, after which the FrdAB

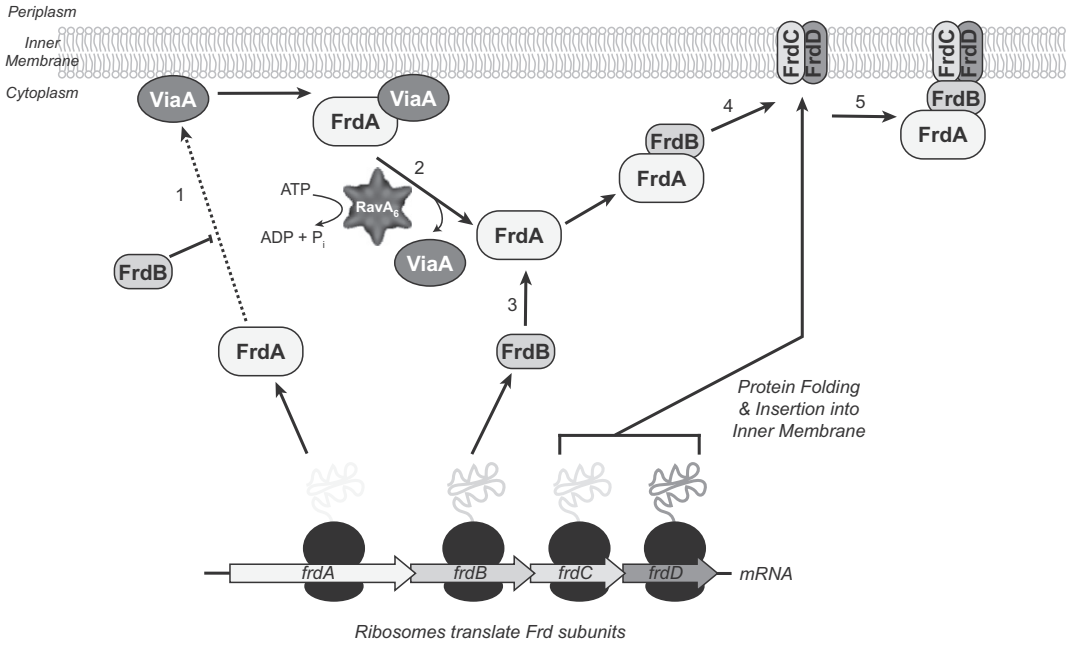

Fig. 7. Model of function of RavA-ViaA in the modulation of the Frd respiratory complex assembly. The Frd complex formation is shown along with the proposed contribution of the ViaA and RavA proteins in regulation of complex assembly. As the Frd operon is translated, the FrdC and FrdD proteins are targeted to the inner membrane, while FrdA and FrdB are processed in the cytoplasm before they associate with the membrane-bound subunits. (1) Free ViaA mainly associates with the bacterial inner membrane where ViaA interacts with FrdA. (2) In the presence of FrdB, ViaA is not observed to associate with FrdA. The ViaA–FrdA interaction is modulated by RavA in an ATP-dependent manner. (3) FrdB associates with FrdA, and (4) this is followed by FrdAB interacting with FrdCD at the membrane to (5) form a functional respiratory Frd complex.

Table 2. List of bacterial strains, plasmids and primers

Bacterial strains	Genotype	Reference
MG1655 (WT)	F-, *rph-1*, *λ*-	[66]
MG1655 Δ*ravAviaA*	MG1655, Δ*ravAviaA*	This study
MG1655 Δ*fnr*::*kan*^{R}	MG1655, Δ*fnr*::*kan*^{R}	This study
MG1655 Δ*rpoS*::*kan*^{R}	MG1655, Δ*rpoS*::*kan*^{R}	This study
PK22	BL21(DE3), Δ*crp-bs990*, *rpsL*, Δ*fnr*, *zcj*-3061::Tn*10*	[34]
DY330 (WT)	W3110, Δ*lacU169, gal490*, *pglΔ8λ*, [*ρ*]cI857 (*cro-bioA*)	[67]
DY330 RavA-SPA	DY330, *ravA-SPA*::*kan*^{R}	This study
DY330 ViaA-SPA	DY330, *viaA-SPA*::*kan*^{R}	This study
DY330 LdcI-SPA	DY330, *ldcI-SPA*::*kan*^{R}	This study
DY330 FrdA-SPA	DY330, *frdA-SPA*::*kan*^{R}	This study
DY330 FrdA-SPA Δ*viaA*::*cat*	DY330, *frdA-SPA*::*kan*^{R}, Δ*viaA*::*cat*	This study
DY330 HemC-SPA	DY330, *hemC-SPA*::*kan*^{R}	This study
DY330 HemX-SPA	DY330, *hemX-SPA*::*kan*^{R}	This study
DY330 CysA-SPA	DY330, *cysA-SPA*::*kan*^{R}	This study
DY330 CysB-SPA	DY330, *cysB-SPA*::*kan*^{R}	This study
DY330 CysI-SPA	DY330, *cysI-SPA*::*kan*^{R}	This study
DY330 CysJ-SPA	DY330, *cysJ-SPA*::*kan*^{R}	This study
DY330 CysM-SPA	DY330, *cysM-SPA*::*kan*^{R}	This study
DY330 CysN-SPA	DY330, *cysN-SPA*::*kan*^{R}	This study
DY330 CysP-SPA	DY330, *cysP-SPA*::*kan*^{R}	This study
DY330 NapA-SPA	DY330, *napA-SPA*::*kan*^{R}	This study
DY330 NapD-SPA	DY330, *napD-SPA*::*kan*^{R}	This study
DY330 NapH-SPA	DY330, *napH-SPA*::*kan*^{R}	This study
DY330 HypA-SPA	DY330, *hypA-SPA*::*kan*^{R}	This study
DY330 HypB-SPA	DY330, *hypB-SPA*::*kan*^{R}	This study
DY330 HypC-SPA	DY330, *hypC-SPA*::*kan*^{R}	This study
DY330 HypD-SPA	DY330, *hypD-SPA*::*kan*^{R}	This study
DY330 HycE-SPA	DY330, *hycE-SPA*::*kan*^{R}	This study
DY330 HycG-SPA	DY330, *hycG-SPA*::*kan*^{R}	This study
EDCM 367 (WT)	MG1655 Δ(P_{lac}-*lacZY*)	[47]
EDCM 367 Δ*fnr*	EDCM 367, Δ*fnr*	This study
BL21 Gold (DE3) pLysS	BL21 (DE3), pLysS(*T7p20 ori*$_{p15A}$)(Cm^R)	Stratagene

Plasmids	Description	***Reference***
p11	Cloning vector derived from pET15b(+)	[68]
pRV	p11-*ravAp-ravAviaA*, for RavA and ViaA overexpression regulated by the native *ravA* promoter	[6]
pR_{K52Q}V	p11-*ravAp-ravA(K52Q)viaA*, for the overexpression of RavA Walker A mutant and wildtype ViaA regulated by the native *ravA* promoter	This study
pPK824	pET11a-*fnrD154A*, for IPTG-induced expression of the mutant FnrD154A	[34]
p11-frdp	p11-*frdp*; *frd* promoter control for similar plasmids carrying genes encoding the subunits of fumarate reductase	This study
pfrdB	p11-*frdp-frdB*, for overexpressing FrdB regulated by the native *frd* promoter	This study
pfrdBCD	p11-*frdp-frdBCD*, for overexpressing FrdB, FrdC, and FrdD regulated by the native *frd* promoter	This study
pETm-60	Cloning vector	[51]
pP_{ravA}-*lacZ*	pETm-60 (*ravAp-lacZ*) for β-galactosidase expression under native *ravA* promoter control	This study
pP_{ravAm1}-*lacZ*	pETm-60 (*ravAp*^{fnr1}-*lacZ*) β-galactosidase expression under control of *ravA* promoter mutant with replacement of the putative Fnr binding sequence, centered at −72.5 from transcription start site	This study
pP_{ravAm2}-*lacZ*	pETm-60 (*ravAp*^{fnr2}-*lacZ*) β-galactosidase expression under control of *ravA* promoter with replacement of the putative Fnr binding site situated at −188.5 from transcription start site	This study
pΔP-*lacZ*	pETm-60 vector backbone with β-galactosidase encoding *lacZ* gene but no promoters	This study
pET3aTr	Cloning vector	[69]
pET3aTr FrdA-SPA	Plasmid for the T7 inducible expression of FrdA-SPA fusion protein	This study
pETm-60 ViaA	Plasmid for the T7 inducible expression of NusA-ViaA fusion protein	This study
p11-RavA	Plasmid for the T7 inducible expression of RavA protein	This study
p11-NTV	Plasmid for the T7 inducible expression of NTV construct	This study
pETm-60 CTV	Plasmid for the T7 inducible expression of NusA-CTV fusion protein	This study

Primer name	Primer sequence (5′ to 3′)
RavA K52Q F	CGCCAGGTATTGCCCAAAGTTTGATCGCC
RavA K52Q R	GGCGATCAAACTTTGGGCAATACCTGGCG
FrdABCD BamHI F	GATTATTATTGGATCCGGCTGCCAGGATGC
frdp NheI R	CATTATTATTGCTAGCCCTCCAGATTGTTTTTATCCCAC
FrdA NheI R	CATTATTATTGCTAGCTCAGCCATTCGCCTTCTCCTTC
FrdB NheI R	CATTATTATTGCTAGCTTAGCGTGGTTTCAGGGTCG
FrdD NheI R	CATTATTATTGCTAGCTTAGATTGTAACGACACCAATCAGCGTG

(continued on next page)

Table 2 (*continued*)

Primer name	Primer sequence (5′ to 3′)
FrdB NheI F	GATTATTATTGCTAGCATGGCTGAGATGAAAAACCTGAAAATTG
FrdB XbaI R	CATTATTATTTCTAGATTAGCGTGGTTTCAGGGTCG
FrdD XbaI R	CATTATTATTTCTAGATTAGATTGTAACGACACCAATCAGCGTG
FrdA BamHI F	ACTGGGATCCGTGCAAACCTTTCAAGCCG
SPA HindIII R	GTCTAAGCTTCTACTTGTCATCGTCATCC
ViaA NcoI F	CATCCCATGGGAATGCTAACGCTGGATACGC
ViaA BamHI R	GTCTGGATCCTTATCGCCGCCAGCGTCTG
NTV NdeI F	ATGCCATATGCTAACGCTGGATACG
NTV BamHI R	ATGGATCCATGTACCACCGGACGTTGC
CTV NcoI F	CATGCCATGGGA AAAGATTACGATGAACAGCC
ravAp NcoI F	ATTCCATGGCACGGCATCGCGTTCAAC
ravAp BamHI R	ATTGGATCCGTGGCGTCCTTTCGTCAAAAG
LacZ BamHI F	ATTGGATCCATGACCATGATTACGGATTCACTG
LacZ NotI R	ATTATTGCGGCCGCGACATGGCCTGCCCGGTT
ravAp(fnrm1) F	CAAAGCTAGCAAACAGAAAAATACCCCCCCTTTG
ravAp(fnrm1) R	GTTTGCTAGCTTTGTGTGGCCGCATTTAGGAGTAC
ravAp(fnrm2) F	GATTGCTAGCAACATGCTCATAGACTAGTCTTTCG
ravAp(fnrm2) R	GATTGCTAGCTTCTTCATTGCCCGCGATTACC
ravApNarLm F	GATTGCTAGCAAAATGCGGCCACATTAACC
ravApNarLm R	GATTGCTAGCCGATTTTGCCGTTAATCGTG

Primer name for EMSA	Primer sequence (5′ to 3′)	Description
ravAp NcoI F	ATTCCATGGCACGGCATCGCGTTCAAC	Forward primer for R-1
ravAp BamHI R	ATTGGATCCGTGGCGTCCTTTCGTCAAAAG	Reverse primer for R-1
ravAp(fnr1-2+) NcoI F	ATTCCATGGTGCTCATAGACTAGTCTTTCGTTGAAATATGAAATG	Forward primer for R-2
ravAp(fnr1-2+) BamHI R	ATTGGATCCAGGAGGAACACACTTTCACCACTTAATG	Reverse primer for R-2
ravAp(fnr1-2-) NcoI F	ATTCCATGGAGAAAAATACCCCCCCTTTGAGAC	Forward primer for R-3
ravAp(fnr1-2-) BamHI R	ATTGGATCCAATAGAAAGGGGACCAAAAACTTCTTCCG	Reverse primer for R-3
fepDp NcoI F	ATTTATTCCATGGCATCATCTGGATCTGCACCG	Forward primer for F-1
fepDp BamHI R	ATTTATTGGATCCGGCCTCCAGCACTACGGAAGCGG	Reverse primer for F-1
hypBp NcoI F	ATTCCATGGCGACGTGTCATTTCGACATCATCGAC	Forward primer for H-1
hypBp BamHI R	ATTGGATCCGACACTGTGGACAGCGGC	Reverse primer for H-1
hypBp(fnr1-2+) NcoI F	ATTCCATGGGGCCGCAAAACACGGCGCAAAAC	Forward primer for H-2
hypBp(fnr1-2+) BamHI R	ATTGGATCCAAACGCGGAATGAGGGTTATGTTCATCACC	Reverse primer for H-2
hypBp(fnr1-2-) NcoI F	ATTCCATGGCGCGGCAGCGTGGCGGAAG	Forward primer for H-3
hypBp(fnr1-2-) BamHI R	ATTGGATCCAATGCAGGTCGCCTTCTTCAGTCTGG	Reverse primer for H-3

cat = chloramphenicol acetyltransferase gene; confers resistance to chloramphenicol; kan^R = kanamycin resistance gene

subcomplex interacts with FrdCD to form the complete Frd complex [18]. The association of RavA-ViaA with FrdA leads to the regulation of the Frd activity as seen in Fig. 6a. We propose that ViaA captures free FrdA to maintain its stability or to allow for the proper covalent attachment of cofactors to FrdA or FrdB proteins before their assembly into the full Frd complex. The association of ViaA with FrdA might also be required to delay the assembly of the FrdAB subcomplex and provide time for the FrdCD subcomplex to form and insert into the inner cell membrane [18].

Such an interactive system of an ATPase and VWA partner has recently been observed in the chemolithoautotroph *Acidithiobacillus ferrooxidans* [44]. The CO_2-assimilating RuBisCo enzyme of *A. ferrooxidans* is activated by the MoxR AAA+ CbbQ protein. Importantly, the VWA domain-containing CbbO protein is required to bind to RuBisCo via the VWA domain to recruit CbbQ to its substrate [44].

Considering that MoxR proteins generally act as chaperones for specific targets [1,2], it is tempting to speculate that RavA-ViaA fulfill this function by regulating the maturation process of specific Frd and Nuo subunits or the assembly of these subunits into respiratory subcomplexes or the assembly of Frd and Nuo complexes into a supercomplex. In this regard, it is interesting to note that the Frd complex works in conjunction with the Nuo complex in the electron transfer from NADH to fumarate during the anaerobic respiration of fumarate [16,18]. In conclusion, the proposed cellular activity of RavA-ViaA adds to a developing pattern of how MoxR AAA+ ATPases might function in nature.

Materials and Methods

Bacterial strains and plasmids

All bacterial strains and plasmids used are listed in Table 2. Primers used in the construction of these strains and plasmids are also listed in Table 2. All KO mutants of the *ravA*/*viaA* ORFs were constructed as previously described [6] by employing lambda red

recombination [45] and P1 phage transduction [46]. EDCM 367 cells were generously provided by Dr. Christophe Merlin (University of Lorraine) [47]. MG1655 Δ*frdA*::*kan*^{R}, MG1655 Δ*rpoS*::*kan*^{R}, and EDCM Δ*frdA*::*kan*^{R} were constructed via P1 phage transduction. The required *frdA* and *rpoS* KO cassettes that carry the *kan*^{R} gene were obtained from BW25113 Δ*frdA*::*kan*^{R} and Δ*rpoS*::*kan*^{R}, respectively, both of which came from the KEIO collection [48,49]. All DY330 strains expressing C-terminal SPA-tagged proteins were a generous gift from Dr. Andrew Emili (University of Toronto) and were constructed using the protocols described in Zeghouf *et al.* [50]. DY330 FrdA-SPA Δ*viaA*::*cat* was constructed by P1 phage transduction. The required *viaA* KO cassette was obtained from MG1655 Δ*viaA*::*cat* that was used in a previous study [6].

The plasmid pRV (p11-*ravAp-ravAviaA*) was constructed as described in our previous work [6]. The plasmid pR_{K52Q}V was generated by QuikChange site-directed mutagenesis (Stratagene) using the primers RavA K52Q F and RavA K52Q R (Table 2). Similarly, for the plasmids pfrdB (p11-*frdp-frdB*) and pfrdBCD (p11-*frdp-frdBCD*), all inserts were PCR amplified using the common forward primer FrdB NheI F (Table 2). The reverse primers FrdB XbaI R and FrdD XbaI R (Table 2) were used for pfrdB and pfrdBCD, respectively. The inserts were then cloned into p11-*frdp* using the restriction enzymes NheI and XbaI (New England Biolabs). All constructs were verified by DNA sequencing.

For high and inducible expression of desired proteins, T7 promoter-controlled constructs (Table 2) were created using common amplification and cloning techniques. Proteins for overexpression include the FrdA-SPA fusion in the pET3aTr vector, NusA-ViaA fusion in the pETm-60 vector, NTV (residues 1–311) in p11, fusion of CTV (residues 312–483) with NusA (NusA-CTV) in pETm-60, and the RavA protein in p11.

The plasmid pP_{ravA}-*lacZ* (Table 2) was constructed with the cloning vector pETm-60 [51]. Expression of *lacZ* is placed under the control of the *ravA* promoter immediately upstream. To construct the plasmid, we first removed a fragment that contains the T7 promoter, *lacI*, and 5′ half of the *nusA* gene in the original pETm-60 using StuI and BglII and the modified vector religated by blunt-end ligation. Next, a 363-bp fragment immediately upstream of the *ravA* ORF, which covers the *ravA* native promoter, was PCR amplified using the primers ravAp NcoI F and ravAp BamHI R (Table 2). The *ravA* promoter was cloned into the modified pETm-60 with NcoI and BamHI. Finally, *lacZ* was PCR amplified from genomic DNA of *E. coli* using the primers LacZ BamHI F and LacZ NotI R (Table 2). The amplified *lacZ* gene was then cloned directly downstream of the *ravA* promoter with BamHI and NotI to give pP_{ravA}-*lacZ*. To generate mutations in the *ravA* promoter in pP_{ravA}-*lacZ*, we used the primers ravAp(fnrm1) F and ravAp(fnrm1) R (Table 2) to replace the consensus *fnr* sequence (5′-TTGCTTATTATCAG-3′) centered at −72.5, with respect to the transcription start site, with 5′-AGAAGC TAGCAACA-3′. Both primers contained the recognition sequence for NheI (5′-GCTAGC-3′), which allowed for digestion and ligation of the PCR product to form circular plasmids. A similar strategy was used to replace putative Fnr recognition site centered at −188.5 (5′-TTAACCTGGCTCAA-3′) with 5′-CAAA GCTAGCAAAC-3′, using the primers ravAp(fnrm2) F and ravAp(fnrm2) R. A 7-nt site centered at −96 (5′-TACTCCT-3′) matching the consensus NarL recognition sequence [39] was replaced with 5′-GCTAGCA-3′ using the primer pair ravAp(NarLm) F and ravAp(NarLm) R.

Protein production and purification

The *E. coli* BL21 Gold (DE3) pLysS (Stratagene) strain was used for high-level expression of desired protein constructs. The NusA-ViaA, NTV, NusA-CTV, RavA, and FrdA-SPA proteins were induced by the addition of 1 mM IPTG to cell cultures grown to mid-log phase at 37 °C. The cultures were grown overnight (~16 h) at 18 °C. After induction, cells were harvested by centrifugation and stored at −80 °C.

Nickel affinity chromatography was performed to purify NusA-ViaA, NTV, NusA-CTV, and RavA constructs, each of which contained a cleavable polyhistidine (6xHis) tag. As the CTV separated from the NusA protein was not soluble, the NusA-CTV fusion protein was stored at −80 °C for further use without removing the NusA-tag. TEV protease was used in a 1:20 M ratio to cleave the 6xHis-tags from NTV and RavA proteins and to remove the NusA (containing the 6xHis tag) moiety of the NusA-ViaA fusion. Additionally, ion-exchange chromatography with Mono S 5/50 HR or Mono Q 5/50 HR columns was performed to further purify RavA and NTV samples, respectively. ViaA protein was separated from NusA using the HiTrap Heparin HP column.

SEC

For SEC, the Superose 6 10/300 GL column (GE Healthcare) was used for RavA, ViaA, and FrdA proteins. The Superdex 200 10/300 column (GE Healthcare) was used for the NTV and NusA-CTV constructs. Proteins were run in the SEC buffer: 25 mM Hepes (pH 7.5), 300 mM NaCl, 1 mM $MgCl_2$, 1 mM DTT, and 5% (vol/vol) glycerol. Elution fractions were collected and visualized using SDS-PAGE.

Co-expression profiling of *ravA* and *viaA* in *E. coli*

The expression levels of *ravA* and *viaA* were compared across different experimental conditions to identify genes with similar expression profiles. To

this end, a large compendium composed of 445 microarray datasets was obtained from the M3D public database (Build 4 of *E. coli* expression data) [52]. These data were available in the form of Robust Multi Array (RMA) normalized profiles [53], which enable the direct comparison of the expression profiles of different protein-encoding genes across multiple experimental conditions. The Pearson correlations, used for comparing the similarity of expression profiles, were computed for all 4125 genes present on the Affymetrix chip against both *ravA* and *viaA*. This allowed the identification of genes that exhibit the most similar expression profiles to the seed set of genes. Due to the large number of conditions in the compendium, a conservative cutoff of 0.5 was adopted as the correlation threshold to identify the functional links to the seed genes. All functional annotations were obtained from publicly available online databases, such as EcoCyc [54], UniProtKB [55], and RegulonDB [56].

Expression analysis of RavA and ViaA in *E. coli* under aerobic and oxygen-limiting conditions

E. coli MG1655 WT, Δ*fnr*::*kan*^{R}, Δ*rpoS*::*kan*^{R}, and Δ*ravAviaA* were grown in LB media (10 g/L bacto-tryptone, 5 g/L yeast extract, and 10 g/L sodium chloride) at 37 °C either aerobically in 200-mL culture flasks with vigorous shaking or under oxygen-limiting condition in 60-mL disposable syringes sealed with sterile end caps with gentle agitation. All cultures were inoculated with single colonies grown overnight on LB-agar plates. Growth of cells was tracked by monitoring the changes in OD_{600} at specific time points. For each time point, an aliquot of the cells was harvested by centrifugation and flash-frozen in liquid nitrogen until use. To determine the levels of RavA and ViaA proteins in cells, we thawed on ice the cell pellets collected and then resuspended them in 0.1 M potassium phosphate (pH 7.5) supplemented with 0.1 M sodium chloride. The volume of each sample was adjusted to give a final cell count of approximately 3.8×10^9 cells/mL as determined by OD_{600}. Cells were lysed by sonication, followed by treatment with 4× SDS-PAGE sample buffer [200 mM Tris–HCl (pH 6.8), 8% SDS, 0.4% bromophenol blue, 40% glycerol, and 400 mM β-mercaptoethanol], and separated on 10% or 12% polyacrylamide gels. The levels of RavA and ViaA were analyzed by Western blotting. A 70-kDa cross-reacting band in the α-ViaA blot was used as the loading control.

EMSA

The *E. coli* Fnr mutant, Fnr_{D154A}, was expressed from the plasmid pPK824 (pET11a-fnr_{D154A}) in strain PK22 lacking fnr (Table 2) and purified as described in Ref. [34], except that SP Sepharose (GE Health Sciences) was used in place of BioRex-70 during the first round of purification. Fnr_{D154A} was used in this assay because it retains the same specificity and affinity as WT Fnr for binding to the Fnr consensus DNA sequence even under aerobic conditions [34]. All DNA substrates required were PCR amplified using the appropriate primers listed in Table 2.

To detect the binding of Fnr_{D154A} to the DNA substrates, we incubated 3 nM of DNA substrate with 60 nM Fnr_{D154A} in 20 mM Tris–acetate (pH 7.5) supplemented with 40 mM KCl, 1 mM $MgCl_2$, and 5% (vol/vol) glycerol for 30 min at 37 °C. All samples were electrophoresed at 4 °C in a 4% polyacrylamide native gel supplemented with 10% polyethylene glycol with 20 mM Tris–acetate (pH 8.0) as the running buffer. The gel was then incubated in 20 mM Tris–acetate (pH 8.0) supplemented with the RedSafe DNA stain (Chembio) with gentle agitation at room temperature to stain the DNA bands contained within. Visualization of the DNA bands was done using the GelDoc 2000 (BioRad).

β-galactosidase reporter assay

To quantify the effect of Fnr on the recognized regulatory sequences in the RavA-ViaA promoter region, we monitored *lacZ* expression under the control of the native and mutated *ravA* promoter using previously established protocols [57]. The pP_{ravA}-*lacZ* plasmid (Table 2) that expresses *lacZ* under the control of the native *ravA* promoter, a no-promoter control (pΔP-*lacZ*), promoter with mutated Fnr recognition sites (pP_{ravAm1}-*lacZ and* pP_{ravAm2}-*lacZ*), or a mutated NarL consensus matching sequence (pP_{ravAm3}-*lacZ*) was constructed as described above. These plasmids were introduced into the EDCM 367 (*E. coli* MG1655 *lacZ*$^-$, *lacY*$^-$), and pP_{ravA}-*lacZ* was also transformed into EDCM 367 Δ*fnr*.

Cells were inoculated from overnight starter cultures and then grown under oxygen-limiting condition in LB supplemented with 1% (vol/vol) glycerol and 50 mM sodium fumarate in sealed and sterilized tubes. The cultures were grown until their OD_{600} reached ~0.5; at which point, three 1-mL samples were collected for each culture. The cells were pelleted and lysed using the permeabilization solution (0.8 mg/mL cetyl trimethyl ammonium bromide, 0.4 mg/mL sodium deoxycholate, 100 mM Na_2HPO_4, 20 mM KCl, 2 mM $MgSO_4$, and 5.4 μL/mL β-mercaptoethanol). The substrate solution (1 mg/mL ortho-nitrophenyl-β-galactoside, 60 mM Na_2HPO_4, 40 mM NaH_2PO_4, 20 μg/μL cetyl trimethyl ammonium bromide, 10 μg /mL sodium deoxycholate, and 2.7 μL/mL β-mercaptoethanol) was added to the lysed samples, and the reaction was run for no more than 120 min. Then, 700 μL of 1 M sodium carbonate was added to stop the reaction after sufficient color had developed. The samples were centrifuged to remove cell debris, and 200 μL of supernatant was

then transferred to a 96-well plate. The absorbance at 420 nm was measured. Miller units were calculated using the following formula [46]:

$$\text{Miller units} = 1000 \times [(\text{Abs}_{450})/(\text{OD}_{600} \times \text{cell culture volume used in mL} \times \text{reaction time in minutes})]$$

Immunoprecipitation by SPA-tagged bait proteins

Endogenous SPA tagging of proteins was carried out in *E. coli* DY330 using the protocols described in Zeghouf *et al.* [50]. Cells with confirmed incorporation of the SPA tags at the C terminus of targeted proteins were grown in LB media at 30 °C in sealed and sterilized 50-mL centrifuge tubes for over 24 h. Cells were then harvested by centrifugation at 4 °C and resuspended in buffer A [25 mM Tris–HCl (pH 7.5), 100 mM KCl, 10 mM $MgCl_2$, 1 mM $CaCl_2$, 0.2 mM EDTA, 1% Triton X-100, 10% glycerol, and 0.5 mM DTT] supplemented with 1 mg/mL lysozyme (BioShop) and 0.1 U/mL DNaseI (Fermentas). After incubation on ice for 15 min, cells were lysed by sonication. Total soluble proteins were isolated from the crude cell lysate by centrifugation. The SPA-tagged proteins and the stably associated proteins were purified using ANTI-FLAG M2 Affinity Beads (Sigma-Aldrich) following the manufacturer's protocols, which were then analyzed by SDS-PAGE and Western blotting.

C-terminally SPA-tagged FrdA was also used as bait to verify interactions with purified proteins. An FrdA-SPA fusion construct, under the control of a T7 promoter in the pET3aTr plasmid, was induced using IPTG in BL21 Gold (DE3) pLysS cells. The expression was carried out for 16 h at 18 °C. Cells were harvested and resuspended in the lysis buffer mentioned above and lysed by sonication. After the removal of cell debris, the supernatant collected from 1 mL of culture was incubated with 40 µL of ANTI-FLAG M2 affinity beads overnight at 4 °C. The beads were placed in Bio-Spin® chromatography columns, and unbound protein was washed away with 5 mL of buffer A. Next, 200 µL of buffer, containing one of the following: 1 µM RavA, 1 µM ViaA, 1 µM NTV, 0.1 µM NusA-CTV, or 0.1 µM NusA, was added to the beads and incubated with gentle shaking for 4 h. The beads were again washed to remove unbound protein. Elution was performed overnight to release FrdA-SPA from the beads by incubation of beads in buffer A containing 200 µL of 0.1 mg/mL TEV protease.

CD spectroscopy

The NTV protein was prepared at 0.4 mg/mL in CD buffer [25 mM Hepes (pH 7.5) and 50 mM NaF]. We used 200 µL of sample with a 1-mm path length quartz cuvette. The Jasco J-810 spectropolarimeter was used for measurement. For the thermal melt profile, the ellipticity was measured at 222 nm from 20 °C to 80 °C as temperature was increased by 1 °C/min. Wavelength scans were performed at 5 °C intervals from 250 nm to 200 nm at a 1-nm pitch and a speed of 50 nm/min. Wavelength scans were performed in triplicate and averaged. The curves were twice smoothened using the Savitzky–Golay algorithm with a convolution width of 25 [58]. To estimate the secondary structure composition, we utilized the BeStSel single spectrum analysis and fold recognition tool [59].

Western blotting

Samples to be analyzed were first separated using a 10% or 12% SDS-PAGE gels. The protein bands were then transferred onto an Amersham Hybond-P PVDF membrane (GE Healthcare) using the TE77X Semi-dry Transfer Unit (Hoefer Inc.) following manufacturer's instructions. The membrane was then blocked, washed, and incubated with the appropriate antibodies as required, using standard protocols. The polyclonal rabbit antibodies against RavA and ViaA were generated at the Division of Comparative Medicine, University of Toronto. The polyclonal rabbit antibodies against FrdA and FrdB in *E. coli* were generously provided by Professor Joel Weiner (University of Alberta, Edmonton, Canada). The monoclonal mouse antibody against the FLAG tag was purchased from Sigma-Aldrich. Commercially available monoclonal antibody against the calmodulin-binding peptide (EMD Millipore) was used to detect the FrdA-SPA construct, and a NusA monoclonal antibody (EMD Millipore) was used to detect either NusA protein or the NusA-CTV fusion.

Analytical ultracentrifugation

A sedimentation equilibrium run was performed on Beckman Optima XL-A analytical ultracentrifuge. The NTV construct was run at concentrations of 1.0 mg/mL, 0.5 mg/mL, and 0.25 mg/mL in a buffer containing 25 mM Hepes, 300 mM NaCl, and 1 mM DTT. The experiment was run at 4 °C for 27 h each at 14,000 and 16,000 rpm using An-60 Ti rotor. Protein concentrations across the length of the cell were measured using absorbance at 280 nm. Origin 4.1 software was used to analyze the data. The partial specific volume, solvent density, and viscosity were calculated using SEDNTERP [60].

RavA ATPase assay

The ATPase activity of RavA, in the presence or absence of ViaA and its domains, was tested using the ATP/NADH-coupled assay [61]. The ATPase buffer with the following final components was

used: 0.2 mM NADH, 3 mM phosphoenolpyruvate, 4.7 U/mL pyruvate kinase, 7.4 U/mL lactate dehydrogenase, 5 mM $MgCl_2$, 25 mM Hepes, and 50 mM NaCl. The relevant proteins were placed in ATPase buffer with 5 mM ATP. Unless indicated, 0.5 μM of proteins were used. The 150-μL reactions were carried out at 37 °C in a clear 96-well plate on the SpectraMax 340PC384 microplate reader, and absorbance was measured at 340 nm for 20 min at 20-s intervals.

Frd activity assay

E. coli MG1655 WT, *ΔravAviaA*, *ΔravAviaA* + p11, *ΔravAviaA* + pRV, *ΔravAviaA* + $pR_{K52Q}V$, and BW25113 *ΔfrdA*::kan^R were grown under oxygen-limiting condition inside sealed and sterilized containers in EZ-defined rich media [62] supplemented with 1% (vol/vol) glycerol and 50 mM sodium fumarate at 37 °C over 16 h. Cells were then harvested by centrifugation, resuspended in 0.1 M sodium phosphate buffer (pH 7), and lysed by two passages through a French Press (Thermo Spectronic) at 18000 lb/in^2. Cell lysis by French Press generates inside-out membrane vesicles. Cell debris was removed by centrifugation. To isolate the membrane vesicles, we subjected the cleared cell lysate to ultracentrifugation at 150,000*g* at 4 °C for 1.5 h. The pelleted membrane vesicles were resuspended in 0.1 M sodium phosphate buffer (pH 7), flash-frozen with liquid nitrogen, and stored at −80 °C until use.

To measure the activity of endogenously expressed Frd in the isolated inside-out membrane vesicles, we used a modified version of the BV colorimetric assay described in Ref. [63]. Briefly, 0.125 mM (final concentration) BV was first reduced with 1.5 mM (final concentration) $Na_2S_2O_4$ in 0.1 M sodium phosphate (pH 7), followed by the addition of 60 μg/mL of membrane vesicles. To initiate the reaction, we added 20 mM (final concentration) sodium fumarate, and the mixture was homogenized by gentle pipetting to minimize the oxidation of BV by air. Frd activity was tracked by monitoring the loss of the purple color as BV was oxidized in the presence of fumarate. This was done by measuring absorbance at 500 nm of the reaction mixture in a standard 1-cm cuvette using the CARY300 UV-Vis Spectrophotometer (Agilent Technologies). Measurements were taken every second for 3 min at room temperature. Frd activity was calculated using the equation: 1 U = 1 μmol BV oxidized/min, with the extinction coefficient of BV = $7.8 \times 10^3\ M^{-1} \cdot cm^{-1}$ [63]. The results were then normalized to the amount of membrane vesicles used to allow comparison between samples.

Supplementary data to this article can be found online at http://dx.doi.org/10.1016/j.jmb.2016.12.008.

Acknowledgments

K.S.W. is the recipient of a fellowship from the Canadian Institutes of Health Research (CIHR) Strategic Training Program in Protein Folding and Interaction Dynamics: Principles and Diseases (TGF-53910) and a Doctoral Completion Award from the University of Toronto. V.B. is the recipient of the Natural Science and Engineering Science Council of Canada's (NSERC) Postgraduate Scholarship-Doctoral (PGS-D) award and of a Jaro Sodek Award—Ontario Student Opportunity Trust Fund (OSOTF) fellowship from the Department of Biochemistry at the University of Toronto. This work was supported by a grant from the Canadian Institutes of Health Research (MOP-130374) to W.A.H.

Received 20 October 2016;
Received in revised form 5 December 2016;
Accepted 5 December 2016
Available online 12 December 2016

Keywords:
ATPases associated with diverse cellular activities (AAA);
chaperone;
flavoprotein;
respiratory chain;
von Willebrand factor A domain

†K.S.W. and V.B. contributed equally to this work.

Abbreviations used:
VWA, von Willebrand factor A; RavA, *r*egulatory *A*TPase *v*ariant *A*; ViaA, *V*WA *i*nteracting with *A*AA+ *A*TPase; LdcI, lysine decarboxylase; Nuo complex, NADH:ubiquinone oxidoreductase I; Frd, fumarate reductase; WT, wild-type; FAD, flavin adenine dinucleotide; EMSA, electromobility shift assay; KO, knockout; ORF, open reading frame; SPA, sequential peptide affinity; TEV, tobacco etch virus; MW, molecular weight; CTV, C-terminal domain of ViaA; NTV, N-terminal domain of ViaA; SEC, size-exclusion chromatography; CD, circular dichroism; BV, benzyl viologen.

References

[1] J. Snider, W.A. Houry, MoxR AAA+ ATPases: a novel family of molecular chaperones? J. Struct. Biol. 156 (2006) 200–209.
[2] K.S. Wong, W.A. Houry, Novel structural and functional insights into the MoxR family of AAA+ ATPases, J. Struct. Biol. 179 (2012) 211–221.
[3] M. Sutter, E.W. Roberts, R.C. Gonzalez, C. Bates, S. Dawoud, K. Landry, et al., Structural characterization of a newly identified component of alpha-carboxysomes: the AAA+ domain protein CsoCbbQ, Sci. Rep. 5 (2015) 16,243.
[4] M. Bhuwan, N. Arora, A. Sharma, M. Khubaib, S. Pandey, T.K. Chaudhuri, et al., Interaction of *Mycobacterium tuberculosis* virulence factor RipA with chaperone MoxR1 is

required for transport through the TAT secretion system, MBio 7 (2016) e02259.
[5] C.A. Whittaker, R.O. Hynes, Distribution and evolution of von Willebrand/integrin A domains: widely dispersed domains with roles in cell adhesion and elsewhere, Mol. Biol. Cell 13 (2002) 3369–3387.
[6] J. Snider, I. Gutsche, M. Lin, S. Baby, B. Cox, G. Butland, et al., Formation of a distinctive complex between the inducible bacterial lysine decarboxylase and a novel AAA+ ATPase, J. Biol. Chem. 281 (2006) 1532–1546.
[7] M. El Bakkouri, I. Gutsche, U. Kanjee, B. Zhao, M. Yu, G. Goret, et al., Structure of RavA MoxR AAA+ protein reveals the design principles of a molecular cage modulating the inducible lysine decarboxylase activity, Proc. Natl. Acad. Sci. U. S. A. 107 (2010) 22,499–22,504.
[8] P.I. Hanson, S.W. Whiteheart, AAA+ proteins: have engine, will work, Nat. Rev. Mol. Cell Biol. 6 (2005) 519–529.
[9] K.S. Wong, J.D. Snider, C. Graham, J.F. Greenblatt, A. Emili, M. Babu, et al., The MoxR ATPase RavA and its cofactor ViaA interact with the NADH:ubiquinone oxidoreductase I in *Escherichia coli*, PLoS One 9 (2014) e85529.
[10] U. Kanjee, I. Gutsche, E. Alexopoulos, B. Zhao, M. El Bakkouri, G. Thibault, et al., Linkage between the bacterial acid stress and stringent responses: the structure of the inducible lysine decarboxylase, EMBO J. 30 (2011) 931–944.
[11] H. Malet, K. Liu, M. El Bakkouri, S.W. Chan, G. Effantin, M. Bacia, et al., Assembly principles of a unique cage formed by hexameric and decameric *E. coli* proteins, eLife 3 (2014) e03653.
[12] Y.K. Park, B. Bearson, S.H. Bang, I.S. Bang, J.W. Foster, Internal pH crisis, lysine decarboxylase and the acid tolerance response of *Salmonella typhimurium*, Mol. Microbiol. 20 (1996) 605–611.
[13] H.S. Girgis, A.K. Hottes, S. Tavazoie, Genetic architecture of intrinsic antibiotic susceptibility, PLoS One 4 (2009) e5629.
[14] G. Unden, J. Bongaerts, Alternative respiratory pathways of *Escherichia coli*: energetics and transcriptional regulation in response to electron acceptors, Biochim. Biophys. Acta 1320 (1997) 217–234.
[15] C.E. Price, A.J. Driessen, Biogenesis of membrane bound respiratory complexes in *Escherichia coli*, Biochim. Biophys. Acta 1803 (2010) 748–766.
[16] Q.H. Tran, J. Bongaerts, D. Vlad, G. Unden, Requirement for the proton-pumping NADH dehydrogenase I of *Escherichia coli* in respiration of NADH to fumarate and its bioenergetic implications, Eur. J. Biochem. 244 (1997) 155–160.
[17] M. Babu, R. Arnold, C. Bundalovic-Torma, A. Gagarinova, K.S. Wong, A. Kumar, et al., Quantitative genome-wide genetic interaction screens reveal global epistatic relationships of protein complexes in *Escherichia coli*, PLoS Genet. 10 (2014) e1004120.
[18] G. Cecchini, I. Schroder, R.P. Gunsalus, E. Maklashina, Succinate dehydrogenase and fumarate reductase from *Escherichia coli*, Biochim. Biophys. Acta 1553 (2002) 140–157.
[19] T.M. Iverson, C. Luna-Chavez, L.R. Croal, G. Cecchini, D.C. Rees, Crystallographic studies of the *Escherichia coli* quinol-fumarate reductase with inhibitors bound to the quinol-binding site, J. Biol. Chem. 277 (2002) 16,124–16,130.
[20] T.M. Iverson, C. Luna-Chavez, G. Cecchini, D.C. Rees, Structure of the *Escherichia coli* fumarate reductase respiratory complex, Science 284 (1999) 1961–1966.
[21] D.J. Westenberg, R.P. Gunsalus, B.A. Ackrell, G. Cecchini, Electron transfer from menaquinol to fumarate. Fumarate reductase anchor polypeptide mutants of *Escherichia coli*, J. Biol. Chem. 265 (1990) 19,560–19,567.
[22] J.H. Weiner, R. Cammack, S.T. Cole, C. Condon, N. Honore, B.D. Lemire, et al., A mutant of *Escherichia coli* fumarate reductase decoupled from electron transport, Proc. Natl. Acad. Sci. U. S. A. 83 (1986) 2056–2060.
[23] J.H. Weiner, P. Dickie, Fumarate reductase of *Escherichia coli*. Elucidation of the covalent-flavin component, J. Biol. Chem. 254 (1979) 8590–8593.
[24] M.R. Carlson, B. Zhang, Z. Fang, P.S. Mischel, S. Horvath, S.F. Nelson, Gene connectivity, function, and sequence conservation: predictions from modular yeast co-expression networks, BMC Genomics 7 (2006) 40.
[25] F. Luo, Y. Yang, J. Zhong, H. Gao, L. Khan, D.K. Thompson, et al., Constructing gene co-expression networks and predicting functions of unknown genes by random matrix theory, BMC Bioinf. 8 (2007) 299.
[26] M. Costanzo, A. Baryshnikova, J. Bellay, Y. Kim, E.D. Spear, C.S. Sevier, et al., The genetic landscape of a cell, Science 327 (2010) 425–431.
[27] D.A. Hume, K.M. Summers, S. Raza, J.K. Baillie, T.C. Freeman, Functional clustering and lineage markers: insights into cellular differentiation and gene function from large-scale microarray studies of purified primary cell populations, Genomics 95 (2010) 328–338.
[28] K. Salmon, S.P. Hung, K. Mekjian, P. Baldi, G.W. Hatfield, R.P. Gunsalus, Global gene expression profiling in *Escherichia coli* K12. The effects of oxygen availability and FNR, J. Biol. Chem. 278 (2003) 29,837–29,855.
[29] Y. Kang, K.D. Weber, Y. Qiu, P.J. Kiley, F.R. Blattner, Genome-wide expression analysis indicates that FNR of *Escherichia coli* K-12 regulates a large number of genes of unknown function, J. Bacteriol. 187 (2005) 1135–1160.
[30] R. Munch, K. Hiller, A. Grote, M. Scheer, J. Klein, M. Schobert, et al., Virtual footprint and PRODORIC: an integrative framework for regulon prediction in prokaryotes, Bioinformatics 21 (2005) 4187–4189.
[31] A. Chakravarty, J.M. Carlson, R.S. Khetani, R.H.A. Gross, Novel ensemble learning method for *de novo* computational identification of DNA binding sites, BMC Bioinf. 8 (2007) 249.
[32] D.J. Studholme, R. Dixon, Domain architectures of sigma54-dependent transcriptional activators, J. Bacteriol. 185 (2003) 1757–1767.
[33] J. Green, C. Scott, J.R. Guest, Functional versatility in the CRP-FNR superfamily of transcription factors: FNR and FLP, Adv. Microb. Physiol. 44 (2001) 1–34.
[34] B.A. Lazazzera, D.M. Bates, P.J. Kiley, The activity of the *Escherichia coli* transcription factor FNR is regulated by a change in oligomeric state, Genes Dev. 7 (1993) 1993–2005.
[35] S.S. Chenault, C.F. Earhart, Organization of genes encoding membrane proteins of the *Escherichia coli* ferrienterobactin permease, Mol. Microbiol. 5 (1991) 1405–1413.
[36] J.L. Lavrrar, C.A. Christoffersen, M.A. McIntosh, Fur–DNA interactions at the bidirectional *fepDGC-entS* promoter region in *Escherichia coli*, J. Mol. Biol. 322 (2002) 983–995.
[37] Z. Chen, K.A. Lewis, R.K. Shultzaberger, I.G. Lyakhov, M. Zheng, B. Doan, et al., Discovery of Fur binding site clusters in *Escherichia coli* by information theory models, Nucleic Acids Res. 35 (2007) 6762–6777.
[38] S.L. Messenger, J. Green, FNR-mediated regulation of *hyp* expression in *Escherichia coli*, FEMS Microbiol. Lett. 228 (2003) 81–86.

[39] K.L. Tyson, A.I. Bell, J.A. Cole, S.J. Busby, Definition of nitrite and nitrate response elements at the anaerobically inducible *Escherichia coli* nirB promoter: interactions between FNR and NarL, Mol. Microbiol. 7 (1993) 151–157.
[40] M. Babu, G. Butland, O. Pogoutse, J. Li, J.F. Greenblatt, A. Emili, Sequential peptide affinity purification system for the systematic isolation and identification of protein complexes from *Escherichia coli*, Methods Mol. Biol. 564 (2009) 373–400.
[41] D.C. Grainger, H. Aiba, D. Hurd, D.F. Browning, S.J. Busby, Transcription factor distribution in *Escherichia coli*: studies with FNR protein, Nucleic Acids Res. 35 (2007) 269–278.
[42] S. Federowicz, D. Kim, A. Ebrahim, J. Lerman, H. Nagarajan, B.K. Cho, et al., Determining the control circuitry of redox metabolism at the genome-scale, PLoS Genet. 10 (2014) e1004264.
[43] T. King, T. Ferenci, Divergent roles of RpoS in *Escherichia coli* under aerobic and anaerobic conditions, FEMS Microbiol. Lett. 244 (2005) 323–327.
[44] Y.C. Tsai, M.C. Lapina, S. Bhushan, O. Mueller-Cajar, Identification and characterization of multiple rubisco activases in chemoautotrophic bacteria, Nat. Commun. 6 (2015) 8883.
[45] K.A. Datsenko, B.L. Wanner, One-step inactivation of chromosomal genes in *Escherichia coli* K-12 using PCR products, Proc. Natl. Acad. Sci. U. S. A. 97 (2000) 6640–6645.
[46] J.H. Miller, A Short Course in Bacterial Genetics: A Laboratory Manual and Handbook for *Escherichia coli* and Related Bacteria, Cold Spring Harbor Laboratory Press, Plainview, NY, 1992.
[47] C. Merlin, G. Gardiner, S. Durand, M. Masters, The *Escherichia coli* metD locus encodes an ABC transporter which includes Abc (MetN), YaeE (MetI), and YaeC (MetQ), J. Bacteriol. 184 (2002) 5513–5517.
[48] T. Baba, T. Ara, M. Hasegawa, Y. Takai, Y. Okumura, M. Baba, et al., Construction of *Escherichia coli* K-12 in-frame, single-gene knockout mutants: the Keio collection, Mol. Syst. Biol. 2 (2006) 2006.0008.
[49] N. Yamamoto, K. Nakahigashi, T. Nakamichi, M. Yoshino, Y. Takai, Y. Touda, et al., Update on the Keio collection of *Escherichia coli* single-gene deletion mutants, Mol. Syst. Biol. 5 (2009) 335.
[50] M. Zeghouf, J. Li, G. Butland, A. Borkowska, V. Canadien, D. Richards, et al., Sequential peptide affinity (SPA) system for the identification of mammalian and bacterial protein complexes, J. Proteome Res. 3 (2004) 463–468.
[51] V. De Marco, G. Stier, S. Blandin, A. de Marco, The solubility and stability of recombinant proteins are increased by their fusion to NusA, Biochem. Biophys. Res. Commun. 322 (2004) 766–771.
[52] J.J. Faith, M.E. Driscoll, V.A. Fusaro, E.J. Cosgrove, B. Hayete, F.S. Juhn, et al., Many microbe microarrays database: uniformly normalized Affymetrix compendia with structured experimental metadata, Nucleic Acids Res. 36 (2008) D866–D870.
[53] R.A. Irizarry, B. Hobbs, F. Collin, Y.D. Beazer-Barclay, K.J. Antonellis, U. Scherf, et al., Exploration, normalization, and summaries of high density oligonucleotide array probe level data, Biostatistics 4 (2003) 249–264.
[54] I.M. Keseler, J. Collado-Vides, S. Gama-Castro, J. Ingraham, S. Paley, I.T. Paulsen, et al., EcoCyc: a comprehensive database resource for *Escherichia coli*, Nucleic Acids Res. 33 (2005) D334–D337.
[55] M. Magrane, the UniProt Consortium, UniProt knowledgebase: a hub of integrated protein data, Database (Oxford) 2011 (2011) bar009.
[56] S. Gama-Castro, H. Salgado, M. Peralta-Gil, A. Santos-Zavaleta, L. Muniz-Rascado, H. Solano-Lira, et al., RegulonDB version 7.0: transcriptional regulation of *Escherichia coli* K-12 integrated within genetic sensory response units (Gensor units), Nucleic Acids Res. 39 (2011) D98–105.
[57] X. Zhang, H. Bremer, Control of the *Escherichia coli* rrnB P1 promoter strength by ppGpp, J. Biol. Chem. 270 (1995) 11,181–11,189.
[58] A. Savitzky, M.J.E. Golay, Smoothing and differentiation of data by simplified least squares procedures, Anal. Chem. 36 (1964) 1627–1639.
[59] A. Micsonai, F. Wien, L. Kernya, Y.H. Lee, Y. Goto, M. Refregiers, et al., Accurate secondary structure prediction and fold recognition for circular dichroism spectroscopy, Proc. Natl. Acad. Sci. U. S. A. 112 (2015) E3095–E3103.
[60] D. Hayes, T. Laue, J. Philo, Program Sednterp: Sedimentation Interpretation Program, Alliance Protein Laboratories, Thousand Oaks, CA, 1995.
[61] K.N. Kreuzer, C.V. Jongeneel, *Escherichia coli* phage T4 topoisomerase, Methods Enzymol. 100 (1983) 144–160.
[62] F.C. Neidhardt, P.L. Bloch, D.F. Smith, Culture medium for enterobacteria, J. Bacteriol. 119 (1974) 736–747.
[63] P.T. Bilous, J.H. Weiner, Dimethyl sulfoxide reductase activity by anaerobically grown *Escherichia coli* HB101, J. Bacteriol. 162 (1985) 1151–1155.
[64] A. Typas, G. Becker, R. Hengge, The molecular basis of selective promoter activation by the sigmaS subunit of RNA polymerase, Mol. Microbiol. 63 (2007) 1296–1306.
[65] A. Mendoza-Vargas, L. Olvera, M. Olvera, R. Grande, L. Vega-Alvarado, B. Taboada, et al., Genome-wide identification of transcription start sites, promoters and transcription factor binding sites in *E. coli*, PLoS One 4 (2009) e7526.
[66] M.S. Guyer, R.R. Reed, J.A. Steitz, K.B. Low, Identification of a sex-factor-affinity site in *E. coli* as gamma delta, Cold Spring Harb. Symp. Quant. Biol. 45 (1981) 135–140.
[67] D. Yu, H.M. Ellis, E.C. Lee, N.A. Jenkins, N.G. Copeland, D.L. Court, An efficient recombination system for chromosome engineering in *Escherichia coli*, Proc. Natl. Acad. Sci. U. S. A. 97 (2000) 5978–5983.
[68] R.G. Zhang, T. Skarina, J.E. Katz, S. Beasley, A. Khachatryan, S. Vyas, et al., Structure of *Thermotoga maritima* stationary phase survival protein SurE: a novel acid phosphatase, Structure 9 (2001) 1095–1106.
[69] S. Tan, R.C. Kern, W. Selleck, The pST44 polycistronic expression system for producing protein complexes in *Escherichia coli*, Protein Expr. Purif. 40 (2005) 385–395.

Legend for Supplementary Figure

Figure S1. Growth profiles of various MG1655 strains under aerobic & oxygen-limiting conditions

Growth profiles for MG1655 wild-type (WT), *Δfnr*::*kan*^{R} and *ΔrpoS*::*kan*^{R} grown aerobically (black data points) or under oxygen-limiting condition (white data points) in LB over 24 hours.

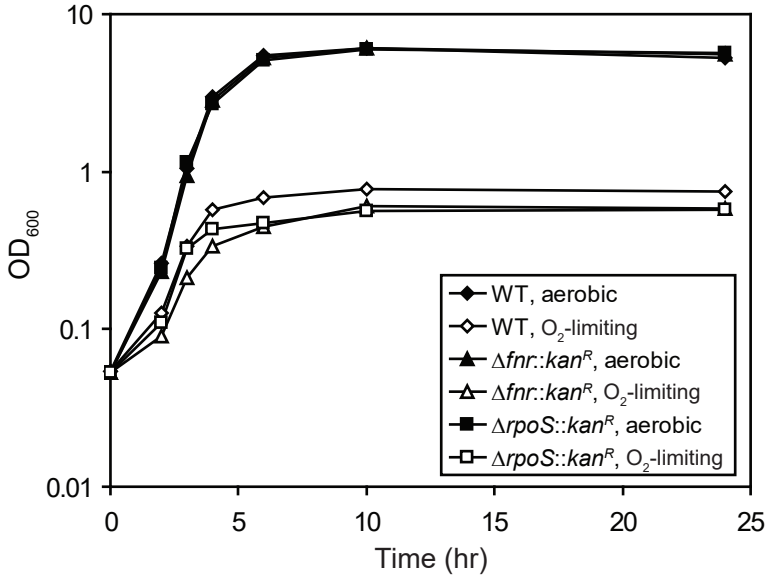
10
1
0.1
0.01
OD600
0
5
10
15
20
25
Time (hr)
WT, aerobic
WT, O2-limiting
Δfnr::kanR, aerobic
Δfnr::kanR, O2-limiting
ΔrpoS::kanR, aerobic
ΔrpoS::kanR, O2-limiting